

**Geochemistry of mafic dikes from the Coastal New England magmatic province in  
Maine, USA and Nova Scotia, Canada**

**William Taylor Whalen**

Thesis submitted to the faculty of the Virginia Polytechnic Institute and State University  
in partial fulfillment of the requirements for the degree of

**Master of Science  
In  
Geosciences**

Mark Caddick  
Esteban Gazel  
James Spotila

May 7<sup>th</sup>, 2019  
Blacksburg, Virginia

*Keywords: geochemistry, mafic dikes, alkaline basalt, Mesozoic intrusives, Triassic  
volcanism, Pangea breakup, Coastal New England magmatic province (CNE), Central  
Atlantic Magmatic Province (CAMP)*

# **Geochemistry of mafic dikes from the Coastal New England magmatic province in Maine, USA and Nova Scotia, Canada**

William Taylor Whalen

## **ABSTRACT**

Mid-Late Triassic-age alkali-basalt dikes were emplaced along the coast of New England between 240-200 Ma. Known as the Coastal New England (CNE) magmatic province, this dike swarm is the immediate magmatic predecessor to the formation of the Central Atlantic Magmatic Province large igneous province at 201 Ma and the breakup of Pangea. The intent of this study is to determine the melt source and mechanisms for melting which produced the Triassic coastal dikes. To achieve this goal, major and trace element compositions were analyzed for 53 CNE dikes from Maine and Nova Scotia. Radiogenic Nd-Sr-Pb-Hf ratios, representing some of the first  $^{176}\text{Hf}/^{177}\text{Hf}$  data for CNE, are reported for 12 of the dikes.

Taken together, the compositional data implicate melting of a deep mantle source that is relatively enriched in incompatible elements, such as a mantle-plume similar to those hypothesized as the source of melting in modern ocean-island basalts (i.e. Hawaii). Dike compositions are inconsistent with melts generated at typical spreading-center ridges (i.e. MORB). Modeling suggests that CNE melts ascended through thick continental crust, consistent with the incipient stages of rifting of Pangea, as evidenced by a heterogeneous mix of melting and crystallization depths, between 0-70km, with no clear geographic pattern. Radiogenic isotope data are relatively consistent and represent a mixture between HIMU, EMI and DMM mantle reservoirs, implying component consisting of relict subducted oceanic crust (or other similarly evolved material). CNE magmatism may have contributed to the breakup of Pangea by destabilizing the lower crust in the limited local area where it erupted, but its true relationship with the breakup of Pangea and later CAMP event requires more study.

# **Geochemistry of mafic dikes from the Coastal New England magmatic province in Maine, USA and Nova Scotia, Canada**

William Taylor Whalen

## **GENERAL AUDIENCE ABSTRACT**

Approximately 200-250 million years ago, hundreds of sheets of lava, called dikes, erupted along what is today the coast of New England. As these volcanic dikes rose up from the Earth's mantle, they traveled along cracks and weak areas of the Earth's crust. Today, these dikes are found along the New England coast as far south as Rhode Island and as far north as Nova Scotia, Canada. Based on the similarity of their geochemistry and petrology, as well as their geologic age and geography of their eruption, geologists group these dikes and similar volcanics together as a single, related magmatic event. This magmatic event produced the Coastal New England (CNE) magmatic province. 250 million years ago, the coast of New England was actually an interior part of the supercontinent known as Pangea. Around 250 m.yr. ago, Pangea slowly began rifting apart, which is when CNE volcanism began. By 200 m.yr. ago, Pangea had broken up, and CNE volcanism had ended. Further complicating the story, a large-igneous province (LIP) also erupted 200 m.yr. ago. Known as the Central Atlantic Magmatic Province (CAMP), this volcanism consisted of enormous volumes of lava that flooded over the entire east coast of the United States. The intent of this study is to determine what geological conditions led to the CNE volcanism. By learning which part of the Earth melted and why, CNE volcanism's role in the breakup of Pangea, and the much larger CAMP eruptions that coincided with it, will become clearer. For instance, did the geologic events that resulted in CNE volcanism contribute to the breakup of Pangea, or did the breakup of Pangea cause CNE volcanism followed by CAMP volcanism? To achieve this goal, the geochemical compositions of 53 CNE dikes from Maine and Nova Scotia were analyzed. Radiogenic Nd-Sr-Pb-Hf ratios for a subset of the dikes (12) were also analyzed. This study presents some of the first radiogenic hafnium data for rocks from CNE.

The data indicate that the melting which produced the CNE dikes began in the deep mantle, similar to the melting of mantle plumes beneath modern ocean-islands such as Hawaii. In contrast, shallow mantle melting, like the melting at mid-ocean ridges where oceanic crust is produced, is not consistent with the geochemical evidence presented for CNE in this study. Modeling suggests that CNE magmas rose through thick continental crust, which caused them to begin forming crystals at relatively high depths. Radiogenic isotope data suggests that part of the mantle that melted was old, recycled oceanic crust or similar mantle material. CNE magmatism may have contributed to the breakup of Pangea by destabilizing the lower crust in the limited local area where it erupted, but its true relationship with the breakup of Pangea and later CAMP event requires more study.

## **DEDICATION**

This study is dedicated to my mother, Cathy Holland, who passed away in 2017 after a sudden and terrible illness. I will miss her always. May she find eternity and worlds beyond.

And to my wife, Lisa Whalen, who has stood with me bravely against many uncertainties and challenges. She has given me strength and inspiration to keep going.

## ACKNOWLEDGEMENTS

Completion of this study would not have been possible without the support and encouragement of the following people (in no particular order):

Virginia Tech Department of Geosciences Faculty and Staff

Esteban Gazel

Mark Caddick

Jim Spotila

Bob Tracy

Steve Holbrook

April Newcomer

Connie Lowe

Georgia Pe-Piper (for Nova Scotia samples)

Luca Fedele (assistance with LA-ICPMS)

Sarah Mazza (assistance with TIMS, XRF)

Michael Bizimis (assistance with TIMS)

Lowell Moore

Lisa Whalen (wife)

Erin Whalen (sister)

Jason Colon (brother-in-law)

Michael Whalen (father)

Cathy Holland (mother)

Richard Ashley (father-in-law)

Daniel Ashley (brother-in-law)

David and Rebecca Brown

Chloe, Cheeto, Gossamer, and Momo (feline contributors)

Mercedes "Mercy" Holland (canine contributor)

Catfish, Jack, Rogue, Toby (lagomorphic contributors)

And the myriad of those deserving my gratitude that I inadvertently neglected to mention.

Thank you, all!

## TABLE OF CONTENTS

ABSTRACT .....	ii
GENERAL AUDIENCE ABSTRACT .....	ii
DEDICATION .....	iv
ACKNOWLEDGEMENTS .....	v
<b>Introduction and geological background.....</b>	<b>1</b>
Mid-late Triassic Alkali-Basalts in New England .....	2
Early Jurassic Central Atlantic Large Igneous Province .....	3
LIPs and Mass Extinctions.....	3
Coastal New England magmatic province and intent of this study .....	3
<b>Materials and Methods.....</b>	<b>4</b>
<b>Results .....</b>	<b>7</b>
CNE Dike Orientations .....	7
CNE Dike Major Elements .....	7
CNE Dike Trace Elements.....	8
CNE Dike Radiogenic Isotopes (Sr-Nd-Pb-Hf).....	8
<b>Discussion.....</b>	<b>9</b>
Summary of previous CNE studies and interpretations.....	9
Interpretations from this study .....	12
Potential for crustal contamination of CNE samples.....	19
Investigating evolution of CNE dike compositions due to crystallization and removal during ascent .....	20
<b>Conclusions.....</b>	<b>24</b>
Future work.....	27
<b>References.....</b>	<b>28</b>
<b>Figures.....</b>	<b>35</b>
Figure 1a-b .....	35
Figure 2 .....	36
Figure 3a-b.....	37
Figure 4 .....	38
Figure 5 .....	39
Figure 6a-b.....	40
Figure 7a-b.....	41
Figure 8 .....	42
Figure 9 .....	43
Figure 10a-d.....	44
Figure 11a .....	45
Figure 11b .....	46
<b>Tables.....</b>	<b>47</b>
Table 1: Dike Locations and Orientation Data .....	47
Table 2: Major Elements.....	48
Table 3: Trace Elements (Sc-Y) .....	49
Table 3 cont.: Trace Elements (Zr-Tb) .....	50
Table 3 cont.: Trace Elements (Dy-U).....	51
Table 4: Radiogenic Isotope Ratios (Nd, Sr, Pb, Hf).....	52

## **Introduction and geological background**

Lithospheric plates at Earth's surface are driven together or apart by plastic flow of flow within the mantle as it cools. Convective cooling of the mantle leads to the creation of new oceanic crust via oceanic spreading ridges. This oceanic crust, initially hot, contracts as it cools over time. Eventually the crust becomes denser than the mantle underlying it and the resulting loss of buoyancy leads to instabilities. Ultimately this leads to subduction, a runaway foundering process which transfers oceanic crust back into the mantle. Subduction at tectonic plate margins eventually removes all intervening thin oceanic crust until thick, buoyant continental lithosphere blocks of subduction-resistant continental crust are joined together to form "supercontinents" (Wilson, 1966; Worsley et al., 1984). Ultimately, the same mantle flow that assembles a supercontinent will split it into the disparate continents consisting of cratons and their accreted terranes. that we know as continents. Evidence suggests this complete process has occurred multiple times in Earth's past (Nance et al., 2014).

The mechanisms of supercontinent breakup are not well understood (Murphy and Nance, 2013). Nevertheless, supercontinents rift due to either passive or active processes (V Courtillot et al., 1999; de Lamotte et al., 2015). Passive rifting occurs when far-field plate motion induces extensional stress (Wortel and Cloetingh, 1986). This stress manifests as rifting along areas of pre-existing weakness, such as a suture resulting from continental collision (Morency et al., 2002) or a pre-existing, regional-scale fault (Boutilier and Keen, 1994). Active rifting occurs when a mantle flow anomaly, such as a plume of deep mantle material (Condie, 1998; Sengör and Burke, 1978) or a localized shallow mantle upwelling (Anderson, 1982), interacts with the lithosphere causing it to weaken and thin. The thinned lithosphere accommodates the rising inflow of hot mantle into the zone of weakness, further eroding the lithosphere and ultimately inducing continuous breakup of the lithosphere (Beniest et al., 2017; Gazel et al., 2012). This breakup may then evolve into a spreading ridge which eventually produces oceanic lithosphere (Koptev et al., 2017). There are still many unknowns with both the active and passive models of

supercontinent breakup and both models are the topic of debate. (Sengör and Burke, 1978; R White and McKenzie, 1989; Hooper, 1990; Storey, 1995).

At least two supercontinents have existed in Earth's past, although there may have been as many as six or more depending on interpretation of the data (Nance et al., 2014). The most recent supercontinent, Pangea, was assembled as of ~290 Ma (Hatcher, 2002). Around 235 Ma, Pangea began to rift along the former eastern Laurentian margin, spatially coincident with the pre-existing Laurentia-Gondwana collisional suture (Hames et al., 2003; Whalen et al., 2015). The rifting of Laurentia and the rest of Pangea was the first stage of Pangea's eventual more extensive breakup (de Lamotte et al., 2015). Thin oceanic lithosphere filled the growing rift between Laurentia and Pangea approximately 65 m.y. after initial rifting began (Schlische et al., 2003). Following separation of Laurentia, Pangea experienced more episodes of plate fragmentation and its breakup has continued through the present day, represented by the continued slow growth of the Atlantic Ocean basin at the mid-Atlantic ridge spreading center (Wilson, 1966).

### **Mid-late Triassic Alkali-Basalts in New England**

Approximately coeval with the initial stages of rifting of Pangea, around ~240 Ma a suite of alkali-basalt dikes began intruding along what eventually became the modern New England coast (Fig. 1a) (Dorais et al., 2005; Pe-Piper and Reynolds, 2000). Erupting between 240 Ma and 200 Ma (Fig. 1b), these dikes span from as far south as Massachusetts to Nova Scotia, Canada, in the north (Fig. 1a) (Dorais et al., 2005; McHone and Butler, 1984; Pe-Piper and Reynolds, 2000). Additionally, similarly aged alkali-basalt dikes found on the other side of the Atlantic may be related those in New England, but official recognition awaits further study (Manspiezer et al., 1978; Manspiezer, 1988). In the United States, the dikes are typically oriented NE-SW (Fig. 2), and run roughly parallel to the modern coastline where they occur. Outcrops of these dikes are most numerous near the coast, but they also occur in limited exposures as far as approximately 100 km inland from the modern coast of New England (Fig. 1a) (McHone and Butler, 1984).

## **Early Jurassic Central Atlantic Large Igneous Province**

Further complicating the story of the initial breakup of Pangea and the aforementioned Triassic-age alkali-basalt dikes, is the 201 Ma onset of large-scale volcanism that formed the Central Atlantic Magmatic Province (CAMP). The CAMP eruptive event produced massive volumes of tholeiitic basalt and andesitic basalt lavas. A total volume of around  $2.3 \times 10^5 \text{ km}^3$  erupted rapidly over an area covering  $10^7 \text{ km}^2$  in less than one million years, CAMP is one of the most extensive large igneous provinces (LIPs) yet identified, with remnant CAMP lavas identified on both sides of the Atlantic on at least four different continents (Fig. 1a) (McHone, 2000; Hames et al., 2003; Blackburn et al., 2013; Whalen et al., 2015). Though rifting between Laurentia and the rest of Pangea was almost complete when CAMP lavas erupted at 201 Ma, formation of the proto-Atlantic ocean crust initiated close to this time (Janney and Castillo, 2001).

## **LIPs and Mass Extinctions**

Most of the major large igneous provinces (LIPs), or at least those with the most prolific eruptive volumes, are linked to continental rifting in Earth's past (V. Courtillot et al., 1999; V. E. Courtillot and Renne, 2003). These major LIP eruptions have been implicated in the elimination of most of the species that lived on Earth at the time of their eruption. The CAMP LIP is no exception, as numerous authors have interpreted it to be an important contributing factor in the T-J mass extinction, one of the largest mass extinctions in Earth's history. The links between the mechanisms of LIP formation, the controls on their eruptivity, and their causal contribution to mass extinctions are not well understood. In the case of the CAMP LIP, we have the advantage of being able to study a magmatic event which precedes and leads into the formation of the CAMP LIP.

## **Coastal New England magmatic province and intent of this study**

Though geographically limited to the New England coast and centered in southeastern Maine (Fig. 1a), the mid-late Triassic-age alkali-basalt dikes emplaced there between 240-200 Ma are the immediate magmatic predecessors to the formation of the CAMP LIP at 201 Ma. The New England dikes share structural, geochemical, and petrologic similarities to each other in addition to their occurrence

within a limited geographic region. Based on those similarities, McHone and Butler (1984) defined the alkali-basalt dikes as comprising a single magmatic province, the Coastal New England magmatic province, hereafter abbreviated to CNE.

The intent of this study is to contribute to the previous work done to describe and interpret the coastal New England magmatic province by contributing new data for 55 of samples from CNE dikes in southeastern Maine. The new data reported here includes major and trace element compositional analyses for all 55 new dike samples, and radiogenic isotope ratios for 12 dike samples. The radiogenic isotope ratios also include  $^{176}\text{Hf}/^{177}\text{Hf}$ , which may be the first time radiogenic Hf is being reported for CNE-related samples, as far as the author is aware. Most of the dikes reported here have not been previously analyzed or described, however nine samples were sourced from an earlier study (Pe-piper and Reynolds, 2000) of CNE-associated dikes in Nova Scotia, Canada. These samples were re-analyzed for comparison with previous work, and one of the older samples was newly analyzed for radiogenic Hf content.

## **Materials and Methods**

For this study, 44 intrusive mafic dikes were sampled for geochemical analyses from outcrops along and adjacent to the coast of Maine, within the bounds specified for the CNE magmatic province by McHone and Butler (1984) (Fig. 1a). Four additional dikes, located north and west of the CNE magmatic province boundary in New Hampshire and Vermont, were sampled and analyzed for comparison with the dikes sampled within the CNE province. An additional nine samples, representing three dikes located in Nova Scotia, Canada, were sourced from an earlier study and were re-analyzed for comparison with previous work (Pe-Piper and Reynolds, 2000). Location data for each dike sample provided in Table 1. All samples were analyzed for whole rock major and trace elements (ME, TE). Twelve of these samples were analyzed for radiogenic isotope ratios for  $^{206}\text{Pb}$ ,  $^{207}\text{Pb}$ , and  $^{208}\text{Pb}/^{204}\text{Pb}$ ,  $^{143}\text{Nd}/^{144}\text{Nd}$ ,  $^{176}\text{Hf}/^{177}\text{Hf}$ , and  $^{87}\text{Sr}/^{86}\text{Sr}$ .

Dike orientation data for the new dikes sampled for this study is summarized in Fig. 2. Orientation data for the Nova Scotia dikes was not re-determined and previously determined orientations

were used if available. For the newly sampled dikes, strike and dip for each dike was measured using a Brunton 8099 Eclipse with a declination set to 15 degrees West of North. Dip angles were determined by taking the average of several clinometer readings of the exposed dike or extant host rock. Precision of these strike and dip measurements is plus/minus 10 degrees.

For major element characterization, bulk rock powder was prepared for each sample and each powder was then processed for whole-rock geochemical analysis of major and trace elements at Virginia Tech following the protocols detail in Mazza et al. (2014). Alteration free (oxides and zeolites etc.) chips were selected using a stereoscopic microscope and the alteration-free chips were subsequently pulverized in an alumina mill. Each of the resulting powders were then combined with ultrapure 34.83%  $\text{Li}_2\text{B}_4\text{O}_7$  – 64.67%  $\text{LiBO}_2$  – 0.5%  $\text{LiBr}$  flux from Spex (certified  $\ll 1$  ppm blank for all trace elements) and cooked the mixture (sample-to-flux ratio 3:1) in a crucible (Pt, 95%-Au, 5%) using a Katanax K1 Prime automated fluxer (1050° C). The resulting homogenous glass discs were loaded into a Panalytical EDS-XRF for major element analysis. USGS standard BHVO-2G was analyzed 10 times as an unknown to determine accuracy and precision during sample analysis. Average accuracy (relative to USGS certified standard reference values for BHVO-2G) was better than 2% for most major elements, however  $\text{MgO}$ ,  $\text{TiO}_2$ ,  $\text{Na}_2\text{O}$  were  $\leq 4\%$ , while  $\text{K}_2\text{O}$  and  $\text{P}_2\text{O}_5$  were within 7%. The average relative standard deviation (RSD %) for 10 runs of BHVO-2G as unknown were  $\leq 1\%$  for all major elements, with the exception of  $\text{Na}_2\text{O}$  at 2%.

Trace element concentrations for the flux-sample glasses were produced using raw counts-per-second (CPS) data obtained at Virginia Tech with an Agilent 7500ce ICP-MS coupled with a Geolas laser ablation (LA) system. Laser ablation was achieved using a spot size of 90  $\mu\text{m}$ , repetition rate of 5 hz, and an energy density of around 7-10  $\text{J}/\text{cm}^2$  per sample. Ablated analyte matter was transported to the ICP-MS using a He flow-rate of around 1 L/min. Flux-sample glass homogeneity was verified by active signal monitoring for select mass numbers during and between collection intervals. To correct for drift, standards were analyzed at the start and end of each run of samples. Final TE concentration data were

reduced using USGS standards BCR-2G, G-2, BHVO-2G and BIR-1a. For 10 runs of USGS standard BHVO-2G, run as an unknown, the average accuracy, relative to standard reference values, was better than 3% for most trace elements, with the exception of Sc, Zr, La, Pr, Yb, Th <4%, and P<sub>2</sub>O<sub>5</sub>, V, Rb, Sr, Ce, Gd <5%. Average precision, expressed as RSD (%), over the same runs was within 3% or better for all elements with the exception of Sc, Sm, Gd, Rb, Er, Hf, Dy, Tm, Th, U 4-5%, Ni, Yb, Ta, Pb <6%, and Lu 8%. Complete LA-ICP-MS procedures outlined in Kelley et al. (2003), Gazel et al. (2012), and Mazza et al. (2014).

Radiogenic isotopes were analyzed at Center for Elemental Mass Spectrometry (CEMS) at the University of South Carolina following the procedures outlined in Bizimis et al. (2013) and Khanna et al. (2014). Powders were used from the same aliquots as those analyzed for major and trace elements. Samples were digested in sub-boiling Teflon-distilled 3:1 HF:HNO<sub>3</sub> (v/v) mixture with the analyses being performed on aliquots of a single digestion. An anion resin was used to separate Pb using HBr and HNO<sub>3</sub> (e.g. Mahnes et al. 1984). A cation resin washed with HCl was used to separate Sr and Nd, which were subsequently purified using a Sr-spec resin and a Ln-resin respectively. Radiogenic ratios were then measured on a Thermo Neptune multi collector ICP-MS with the PLUS upgrade. For Sr radiogenic isotope ratios the NBS-987 Sr standard was determined at  $^{87}\text{Sr}/^{86}\text{Sr} = 0.710329 \pm 0.000007$  (n=7) using  $^{87}\text{Sr}/^{86}\text{Sr} = 0.1194$  for instrumental fractionation correction. All Sr ratios are reported relative to the published value of  $^{87}\text{Sr}/^{86}\text{Sr} = 0.710250$  for the NBS-987 standard to correct for instrument bias. For Nd ratios the JNdi Nd standard was determined at  $^{143}\text{Nd}/^{144}\text{Nd} = 0.512113 \pm 0.000009$  (n = 7) using  $^{146}\text{Nd}/^{144}\text{Nd} = 0.7219$  for fractionation correction. All Nd ratios are reported relative to the published value of  $^{143}\text{Nd}/^{144}\text{Nd} = 0.512115$  for the JNdi standard. Pb isotopic ratios were analyzed using the TI-addition technique (W M White et al., 2000) and the NBS-981 standard (determined at  $^{206}\text{Pb}/^{204}\text{Pb} = 16.9345 \pm 0.008$ ,  $^{207}\text{Pb}/^{204}\text{Pb} = 15.4883 \pm 0.0011$ ,  $^{208}\text{Pb}/^{204}\text{Pb} = 36.6891 \pm 0.0032$  (n=12)). All Pb ratios are reported relative to the published NBS-981 values of Todt (1996):  $^{206}\text{Pb}/^{204}\text{Pb} = 16.9356$ ,  $^{207}\text{Pb}/^{204}\text{Pb} = 15.4891$ ,  $^{208}\text{Pb}/^{204}\text{Pb} = 36.7006$ . For Hf ratios an in-house standard corresponding to the JMC-475 Hf

standard was determined at  $^{176}\text{Hf}/^{177}\text{Hf} = 0.282127 \pm 0.000004$  ( $n = 7$ ) using  $^{179}\text{Hf}/^{177}\text{Hf} = 0.735$  for fractionation correction. All Hf ratios are reported relative to the published value of  $^{176}\text{Hf}/^{177}\text{Hf} = 0.282160$  for the JMC-475 standard. Radiogenic isotope ratios were age corrected to initial eruptive values at 230 Ma assuming current parent/daughter values as reported in Table S1, using decay constants from Steiger and Jäger (1977). Measured radiogenic isotope ratios and errors, as well as calculated initial radiogenic isotope ratios (age-corrected to 230 Ma) radiogenic isotopes are both reported in Table S1.

## Results

### CNE Dike Orientations

The most common dike orientation of the sampled dikes was NE/SW striking with ~30% of dikes striking ~53° azimuth (Fig. 2). Dip angle was 80-90° for most dikes and dip direction for sub-vertical dikes was almost always NW, with the exception of three dikes that dip SE.

### CNE Dike Major Elements

Most samples plot in the basalt and trachy-basalt fields of the total-alkali-silica (TAS) diagram of Le Maitre et al. (1989) (Fig. 3a). Notable exceptions are a few samples from Casco, ME which also plot within the basaltic trachy-andesite, trachy-andesite, and trachyte fields and are close to the boundaries of phono-tephrite, tephri-phonolite, and phonolite respectively. On an Irvine-Barager plot of alkalis vs.  $\text{SiO}_2$  (Irvine and Baragar, 1971) roughly half of the samples plot in the alkaline field and half plot in the subalkaline field (Fig. 3b). Alkaline and subalkaline groups do not show a pattern based on sampling location and most sampling localities presented both alkaline and subalkaline samples. A notable exception is the Bald Cliff location where most of the samples are subalkaline. The  $\text{Mg\#}$  ( $[(\text{Mg}/(\text{Mg} + \text{Fe})) * 100]$ ) for all samples is between 65 and 35 (Fig. 4) and there do not appear to be trends based on sample location, however samples from Nova Scotia and Bald Cliff, ME plot together at higher  $\text{Mg\#}$ 's, between 65 to 56. CaO decreases with decreasing  $\text{Mg\#}$ , although there is some spread on the CaO axis.  $\text{Al}_2\text{O}_3$  generally increases with decreasing  $\text{Mg\#}$ , indicating that the samples are in a cotectic between olivine and clinopyroxene.  $\text{TiO}_2$ ,  $\text{K}_2\text{O}$ , and  $\text{P}_2\text{O}_5$  behave similarly to each other and follow two trends. The first trend

involves a group of outlier samples with relatively higher Mg#'s that correspond with some of the highest TiO<sub>2</sub>, K<sub>2</sub>O, and P<sub>2</sub>O<sub>5</sub> concentrations, but these high Ti, K, and P concentrations occur over a relatively limited Mg# range (55-65). The second, main trend group begins at Mg# 56 and extends to lower Mg#s, generally showing an increase in TiO<sub>2</sub>, K<sub>2</sub>O, and P<sub>2</sub>O<sub>5</sub> as Mg# decreases. The Main Trend group is composed of the rest of the samples excluding the few from the Outlier Trend group and therefore represents the bulk of the CNE dikes analyzed. The samples in the Main Trend group show relatively flat TiO<sub>2</sub> until Mg# 43 where TiO<sub>2</sub> begins to decrease with decreasing Mg#, which may suggest the crystallization and separation of rutile prior to emplacement of the lower Mg# samples in the Main Trend group. Na<sub>2</sub>O generally increases with decreasing Mg# in both groups. In both groups, FeO appears as an inverse of the pattern described for TiO<sub>2</sub>, and the Outlier Trend group (higher Mg#s) contains the lowest samples with the lowest FeO of all. In the Main Trend group, FeO increases from ~10 wt.% to a maximum of ~15 wt.% at Mg# 40.

### **CNE Dike Trace Elements**

On a chondrite-normalized spider diagram of rare-earth element concentrations (Fig. 6a), most of the samples are relatively enriched in light rare earth elements (LREE) relative to the heavy rare earth elements (HREE). La/Yb ratio is between 10 and 20 for most samples, with mean of La/Yb = 15. There is little variation in MREE and HREE between locations in coastal Maine and Nova Scotia. These locations do vary in LREE, although there does not appear to be a pattern. On a pyrolite-normalized spider diagram of select incompatible trace element concentrations (Fig. 6b), samples show the most variation in Pb and K. Pb concentrations for some samples show anomalously low deviations relative to the rest of the data. K concentrations for some samples show anomalously high deviations relative to the rest of the data and these probably represent post-emplacement alteration. One coastal Maine sample (Port-1B) was relatively depleted in all incompatible elements compared to the rest of the data.

### **CNE Dike Radiogenic Isotopes (Sr-Nd-Pb-Hf)**

12 samples (Maine locations: Bald Cliff, Cliff Walk, Casco, Kittery, Ogunquit, Skelton, Lake Sebago, as well as Nova Scotia, and Livermore Falls, NH) were analyzed for Sr, Nd, and Pb and Hf isotopes.  $^{87}\text{Sr}/^{86}\text{Sr}$  ranges between 0.7037-0.7060 (Fig. 7a).  $^{143}\text{Nd}/^{144}\text{Nd}$  ranges from 0.5126 – 0.5129 (Fig. 7a).  $^{206}\text{Pb}/^{204}\text{Pb}$  ranges from 18.783 – 20.142 (Fig. 7b).  $^{207}\text{Pb}/^{204}\text{Pb}$  ranges from 15.6016-15.6868 (Fig. 8).  $^{208}\text{Pb}/^{204}\text{Pb}$  ranges from 38.5871 – 39.6797.  $^{176}\text{Hf}/^{177}\text{Hf}$  ranges from 0.282713- 0.282877 (Fig. 9). CNE isotope ratio data appears to show a mix between modern EMII, DMM, and HIMU mantle radiogenic isotope domains, with several samples showing a relative affinity for HIMU, especially in eNd vs  $^{87}\text{Sr}/^{86}\text{Sr}$  space [radiogenic isotope reservoirs referenced are from Hofmann (2003)]. Radiogenic isotope data from previously published studies of the CNE province generally plot within the range of the new data collected in this study, and our new data expands the range of compositions known to be associated with CNE. (Pe-Piper and Jansa, 1986; McHone, 1992; Pe-Piper et al., 1992; Sundeen and Huff, 1992; Ross et al., 1992; Pe-Piper and Reynolds, 2000; Dorais et al., 2005).

## Discussion

### Summary of previous CNE studies and interpretations

The Coastal New England Triassic dikes were first described in an 1838 survey by Jackson (Hineline, 1988). Subsequent studies of the dikes focused on their mineralogy and petrology (Hitchcock, 1861; Kemp, 1890; Keeley, 1914; Keeley, 1923; Wandke, 1922; Haff, 1939; Haff, 1941; Haff, 1943). Later work focused on structural controls, the dikes' relation to regional geology, and detailed outcrop mapping (Hussey, 1962; Swanson, 1982; Swanson, 1983; Swanson, 1992). In the 1980s studies of the dikes geochemical and petrological properties were published. (McHone and Trygstad, 1982; Bellini et al., 1982; Eby, 1985; Dye, 1985; Jansa and Pe-Piper, 1985; Pe-Piper and Jansa, 1986; McHone et al., 1987; Sundeen and Huff, 1992).

The alkali-basalt dikes in the region were first grouped together as a cogenetic magmatic province by McHone and Butler (1984) wherein they described the general geographic boundaries of the CNE magmatic province and assigned it the name Coastal New England magmatic province (CNE). In the

same work, the authors delineated four separate Mesozoic igneous provinces in the general area of New England and Quebec, of which CNE was one. These provinces, in order of oldest to youngest are the CNE magmatic province (210-240 m.y.), the White Mountain magma series or WMMS (160-200 m.y.), the Eastern North America Dolerite Province or ENA, which is also known as the Central Atlantic Magmatic Province or CAMP (165-200 m.y.), and the New England-Quebec Province or NEQ (95-135 m.y.). They interpreted CNE magmatism as occurring due to pre-rift uplift of the region and subsequent initial rifting of Pangea.

Hermes et al., (1984) describe several Triassic alkali and transitional basalt dikes with similar geochemistry and ages to the ME CNE dikes in eastern Massachusetts and Rhode Island. Their interpretation is that they are the result of very low degrees of partial melting a depth and may represent rift-flank, as opposed to rift-axial, magmatism. Several dikes with geochemistry and ages similar to the CNE dikes of southeastern Maine were discovered during offshore drilling in the Northumberland Strait, Canada and were interpreted as relating to the CNE dikes known then in New Hampshire (Pe-piper and Jansa, 1986).

McHone (1992) further refined the geographic boundaries of CNE and published new geochemical analyses for several CNE related dikes in coastal Maine. Based on detailed outcrop mapping of the CNE dikes in Maine, Swanson (1992) interpreted the CNE province to be 500-km-long, north-northeast-trending zone of crustal extension running from central Maine to Rhode Island, representing an early stage of continental rifting in New England that continued into the Jurassic. The portion of the CNE province that extends into coastal New Hampshire was studied by Sundeen and Huff (1992), who reported that there are at least 100 outcrops of alkali basalt dikes with similar petrology and orientations (average strike 055) to the CNE dikes in southeastern Maine, and compositional analyses and age dating of two of the NH CNE dikes confirms that they have similar geochemistry and K-Ar ages (~220 Ma) to the dikes from southeastern Maine.

Work by Ross et al. (1992) in Massachusetts indicated the presence of alkali basalt dikes with similar geochemistry to the CNE dikes of southeastern Maine and interpreted the MA dikes as having been emplaced starting at the onset of continental rifting in the mid-Triassic. The MA CNE dikes were also reported as striking generally northeast-southwest, in agreement with the other CNE dikes. Ross et al. (1992) attributed the abundance of alkali basalt dikes in MA, combined with the absence of coeval tholeiitic basalt dikes to implicate their origin as rift-flank related magmatism, whereas tholeiitic basalts would be expected for rift-axial magmatism.

CNE-related lamprophyre (alkali basalt) dikes were reported from southwest Nova Scotia, Canada, based on ages of 222-230 Ma and similar major and trace element whole-rock geochemistry (Pe-piper and Reynolds, 2000). Trace element composition and radiogenic isotope data for these Nova Scotia CNE dikes indicated that they were likely produced by a small degree of partial melting of enriched mantle, and melting was due to decompression due to the incipience of continental rifting or related to the thermal effects of adjacent emplacement of anomalously hot mantle material, such as the arrival of a mantle plume. The Nova Scotia CNE dike samples analyzed in the current work are the same samples from Pe-piper and Reynolds (2000). They were graciously loaned by Georgia Pe-piper for re-analysis and interpretation.

In one of the first studies to focus on comparing the geochemistry of CNE and CAMP, Dorais et al. (2005) compared the tholeiitic flood basalts representative of CAMP magmatism and the alkali basalt dikes of CNE. They confirmed some of the distinct differences in trace element composition of the two magmatic suites that had previously been noted in some earlier studies and interpreted the differences to be due to distinct mantle sources for each event. They bolstered that interpretation by presenting radiogenic isotope ratio measurements that showed CNE alkali basalts overlap with the field comprised of other ocean-island basalts (OIB), while CAMP tholeiitic basalts plotted closer to enriched mantle and continental flood basalts, due primarily to higher radiogenic  $^{87}\text{Sr}/^{86}\text{Sr}$  in CAMP than CNE. The same distinction is noted in the results of the current study in Fig. 7a. Dorais et al. (2005) interpreted the CNE

alkali basalts as having melted at a greater depth than CAMP tholeiitic basalts and potentially representing melting similar to OIB pre-shield-stage plume-related melting seen today in the Loihi Seamount of the Hawaiian Islands.

## **Interpretations from this study**

### CNE Dike Orientations

Swanson (1992) obtained an average strike of 055 for the CNE dikes in that study, and interpreted the average 055 strike and steep (near-vertical) dip angles of the CNE dikes in Maine to be controlled by the bedding of the host rock there, which strikes at 060 with a near-vertical dip. Similarly, in New Hampshire, Sundeen and Huff (1992) reported that the strike of the CNE-related dikes there followed the strike and dip of the foliation planes of the metamorphic host rock, which dip steeply and strike ~045. The predominant orientation of the CNE dikes sampled for this study is ~055 degrees (Fig. 2) with a steep, near-vertical dip, and these orientations agree with previous work from Maine and other states.

Dike swarms oriented parallel to each other are commonly associated with crustal rifting. These dike swarms are structurally controlled by the direction of extensional stress experienced by the crust and tend to erupt along faults and other planes of weakness (Odé, 1957, Muller and Pollard, 1977, Nakamura, 1977). In the case of CNE, the parallel orientation of the dikes alone might indicate that melting occurred due to crustal rifting, but geochemical evidence suggests they are not the result of crustal melting, extensional or otherwise, so another explanation is required for the observed orientations of CNE dikes. Aside from rift-related volcanism, CNE may represent intraplate volcanism caused by melting of an ascending mantle-plume. Mantle-plume ascent and interaction with the overriding lithosphere is typically associated with crustal doming and uplift, which produces hypabyssal-to-surficial dike swarms that radiate from a central locus coincident with the center of domal uplift (Chadwick Jr and Dieterich, 1995, Gudmundsson and Sambridge, 1998). Although a radiating dike swarm pattern is typical of mantle-plume related volcanism, the radial pattern may not occur if the crust is too thick or if pre-existing structural

features provide easy access for dikes to ascend from the zone of melting (Ernst et al., 2001). Therefore, domal uplift that would have been caused by ascending plume material during CNE magmatism may have been inhibited by the thickness of the overlying continental crust, which was likely overthickened due to continent-continent collision during the assembly of Pangea (Hatcher, 2002). As noted by previous authors, the most likely alternative explanation for the lack of obvious radiating dike swarms in the CNE magmatic province is that during ascent through the crust, pre-existing structural features of the host rock, such as bedding or foliation planes, may have strongly controlled the regional character of dike orientation during intrusion and emplacement.

#### CNE Major and Trace Element Compositions

The total-alkali-silica (TAS) plot (Fig. 3a) indicates that lithology of most of the dikes sampled in this study are basaltic, with a subordinate population of alkalic (trachybasalt and basaltic trachyandesite). As pointed out in previous work, alkalic volcanism is typically associated with post-shield stage, intraplate ocean-island magmatism, but may also be associated with pre-shield stage ocean-island magmatism as well (Dorais et al., 2005). In the case of CNE, degree of partial melting and/or depth of the onset of magma crystallization may have been influenced by the character of the convergent margin of Pangea and the resulting overthickened lithosphere. Ratios of middle rare earth elements (MREE) and heavy rare earth elements (HREE), exemplified by Sm/Yb, can help identify melt/crystallization effects in magmatic suites (Pearce, 2008). Plotted against the ratio of Mg vs total Mg and Fe (Mg#), a magmatic suite evolving from a primary magma should display increasing Sm/Yb as Mg# decreases (Pearce, 2008). In CNE, most of the dikes sampled show this trend (Fig. 4), however some relatively high Sm/Yb outliers at high Mg# exist. These same outliers are also noted in the results section of this study, referenced as the Outlier Trend group. As many of these outliers are from the Nova Scotia CNE dikes (triangles in Fig. 4), this may indicate a limited zone of enrichment in the mantle source (plume or otherwise) in that area.

When incompatible trace elements concentrations are normalized against chondrite reference values and plotted logarithmically in a “spider” diagram, trends can be identified that repeat in rocks from

similar tectonic settings. For example, mid-ocean ridge basalts are the product of relatively high-degrees of partial melting (up to 20%). As a result, the patterns they display in the most relatively incompatible rare-earth elements (REE) curve downward, to the left (Fig. 6a), with a magnitude of 10x that of chondrites. Contrasting that, ocean-island basalts (OIB), especially alkalic OIB, are typically the result of relatively low (1-2%) degrees of partial melting (Takahashi and Kushiro, 1983), and the most incompatible rare-earth elements in those rocks are 50-100x that of chondrites, forming a slope down toward the right side of the spider diagram (Fig. 6a). These trends are the result of preferential enrichment of OIB, relative to MORB, of incompatible trace elements due melt/crystallization mechanisms during magma generation. CNE samples most closely follow the trend of other, typical OIB, which is a strong indication that they are also generated by potentially low fraction melting of relatively un-depleted mantle, as is interpreted for modern OIB and have often been genetically linked to hotspot/plume activity (Sun and McDonough, 1989; A Hofmann, 1997). For additional contrast, CAMP samples closely resemble trends found in typical lower-crust samples, indicating that CNE and CAMP have different sources and mechanisms of melt generation (Dorais et al., 2005; Whalen et al., 2015).

The presence of sloped REE patterns for CNE dikes on a chondrite-normalized “spider” diagram indicates that CNE melts came from a garnet-bearing source. Garnet retains Yb and heavy REE (HREE) preferentially over light and middle REE (LREE and MREE) (Hoal et al., 1994; Pearce, 2008). If garnet is present in the source of melting, it fractionates LREE and MREE from HREE, causing sloped REE patterns similar to those observed for CNE dikes (Fig. 6a). If garnet is not present in the source of melting, REE patterns (particularly for MREE and HREE) are much less sloped, appearing somewhat flat. A small population of CNE dikes have less fractionated MREE vs HREE than the rest of the sample set and these dikes may reflect melts derived from a garnet-free source.

Since garnet is implicated in the source for most CNE melts, a rough estimation of depth for melt generation can be made. Garnet stability fields for different mantle lithologies vary due to compositional differences. In peridotite lithologies, garnet is only stable only at pressures of ~2.3 GPa or more (at

temperatures of 1100 degrees Celsius or higher), whereas with pyroxenite lithologies, garnet is stable at lower pressure and temperature, ~1.2 GPa or more (at temperatures of 1100 degrees Celsius or higher) (O'Hara et al., 1971; Hirschmann and Stolper, 1996). Therefore, depending on melt source lithology, most CNE melts appear to have been generated between at depths of at least ~40km or more if the source is dominantly pyroxenitic, or ~80 km or more if the source is dominantly peridotitic.

Incompatible trace elements other than the rare-earth elements display similar patterns to those in the REE spider diagram (Fig. 6a), but some additional context can be ascertained due to the chemical properties of certain elements. Large-ion lithophile elements (LILE) are typically fluid-mobile, meaning fluids may be enriched in these elements, or that rocks/minerals may be leached by fluids with low concentrations of LILE (Pearce and Peate, 1995). In the case of CNE, most samples were not preferentially enriched in LILE, though a few had high Pb (positive excursion in blue field, Fig. 6b). A similar spike in Pb can be seen in trace element patterns of lower crust, and the few CNE samples with high Pb may have assimilated more country rock during ascent, leading to higher Pb content. The counter-argument to this hypothesis is that other LILEs, such as K and Sr, are not similarly enriched in the CNE samples that are high in Pb. Certain high field-strength elements (HFSE) are typically compatible in specific mineral phases, such as Nb and Ta in rutile (McDonough, 1991). The relative enrichment or depletion in bulk-rock Nb and Ta can indicate whether rutile was consumed during melt generation. Subduction zone-related magmas are often relatively depleted in Nb and Ta, whereas OIB are mildly enriched in Nb and Ta, implying rutile stability in subduction zone melting regions (McDonough, 1991). CNE dike samples all show relative enrichment in Nb and Ta, whereas CAMP and lower-crust samples display Nb and Ta depletion common to subduction-zone related magmas and other melts sourced from rutile-stable protoliths (Fig. 6b). This difference in HFSE between CAMP and CNE further supports the idea that both magmatic suites have different sources and different mechanisms of melt generation.

#### CNE dike radiogenic isotope ratios discussion

CNE dike samples plot nearest, but adjacent to samples from the Cape Verde islands OIB. In  $eNd$  vs  $^{87}Sr/^{86}Sr$  space, CNE samples, age-corrected to 230 Ma, plot between HIMU and EMI (Fig. 10a). Calculated mixing lines between HIMU and EMI are able to reproduce CNE samples (Fig. 10a). In  $^{206}Pb/^{204}Pb$  vs  $^{87}Sr/^{86}Sr$  space, CNE samples plot between HIMU, DMM, and EMI (Fig. 10b). Calculated mixing lines between HIMU and EMI are able to reproduce CNE samples (Fig. 10b). In  $^{206}Pb/^{204}Pb$  vs  $^{207}Pb/^{204}Pb$  space, CNE samples plot between HIMU and EMI (Fig. 8). Calculated mixing lines between HIMU and EMI are not able to reproduce CNE samples (Fig. 10d). In  $eNd$  vs  $eHf$  space, CNE samples plot closest to HIMU, and they plot lower than all other OIB (Fig. 9). Calculated mixing lines between HIMU and EMI are able to reproduce CNE samples (Fig. 10c).

#### Mantle isotope domains discussion and interpretation from literature

Analyses of thousands of mafic rocks for radiogenic isotope ratios from all over the globe have revealed systematic trends, leading to the labeling of specific ranges of radiogenic isotope ratios that represent extreme compositional endmembers. Although many potential endmembers have been identified, only a few of the most commonly cited mantle isotope reservoirs will be treated here, namely DMM, FOZO, HIMU, EM1, and EM2.

#### FOZO

FOZO is interpreted to be a commonly shared source reservoir among most OIB. FOZO stands for focal zone, and most OIB magma suites form a trend between FOZO and another mantle reservoir.

#### DMM

All mid-ocean ridge basalts possess a strong DMM (depleted MORB mantle) component, which means they plot in a relatively less radiogenic area of isotope ratio graphs. Mid-ocean ridge basalts (MORB) show relative depletions in incompatible trace elements that indicate they are sourced from an upper mantle layer that has experienced extensive melt extraction prior to MORB melting. This is confirmed by relatively high radiogenic Nd ratios, which indicate that the mantle source of MORB have

been enriched in Sm compared to Nd. This depleted MORB mantle (DMM) source appears to be relatively homogenous and underlies most of the Earth's crust. This means that the DMM reservoir signature may be found in both oceanic intraplate signatures, where it accompanies relatively trace-element enriched sources, such as HIMU or EM1, as well as continental intraplate signatures.

### HIMU

HIMU is a mantle reservoir endmember seen in samples from the Austral, Cook, and St. Helena islands OIB. HIMU is popularly hypothesized to be recycled oceanic crust that has been relatively depleted in alkali elements and Pb as a result of hydrothermal alteration and selective leaching of large-ion lithophile elements (LILE) by fluid dehydration during subduction (Sobolev et al., 2007). Alternative hypotheses include the metasomatization of oceanic lithosphere by low-degree partial melts that are preferentially enriched in U and Th (Sun and McDonough, 1989).

### EM1

EM1 (enriched mantle I) is a mantle reservoir endmember seen in samples from the Pitcairn, Gambier, and Tristan islands OIB. Several explanations for EM1 have been proposed, including, recycling of delaminated SCLM, recycling of ancient subducted continental crust sediments, or recycling of the lower crust. Lower crust is eroded from continental margins during subduction of oceanic crust and this tectonic erosion provides a mechanism for lower crust to enter the mantle and be recycled (Willbold and Stracke, 2006).

### EM2

EM2 (enriched mantle II) is a mantle reservoir endmember seen in samples from the Society, Samoa, and Marquesas islands OIB. EM2 may represent subducted continental crust, metasomatized mantle, recycled oceanic crust accompanied by minor amounts of continent crust sediment, or recycled melt-impregnated oceanic lithosphere. A recycled sedimentary signature appears to be necessary to duplicate the EM2 flavor, but the sedimentary signature is not recycled from within the deep mantle.

Instead, the sedimentary signal may be due to contamination of mantle plume melts as they ascend through the lithospheric mantle or crust (Bohrson and Reid, 1995).

#### Implications of mixing between HIMU-EM1 and DMM in CNE dikes

Age corrected radiogenic isotopes for CNE rocks in this study appear to represent a mix of HIMU-EM1 and some DMM. This is especially apparent for Nd, which is relatively low compared to Nd for other OIB. Hart and Zindler (1986) suggested that proposed that data from certain oceanic islands (Walvis Ridge, San Felix, Comores, New England Seamounts, St. Helena, and Tubuaii) form an array where all locations share relatively low radiogenic Nd (LoNd) isotope ratios. Their interpretation was that samples on this 'LoNd' array could be explained as physical mixes of HIMU and EM1 endmembers, and LoNd-adjacent samples explained as HIMU-EM1 mixed reservoir melts that then mixed with melts from another mantle reservoir, such as DMM. In their model, the HIMU reservoir is sub-continental lithospheric mantle (SCLM) that has been metasomatized during preceding subduction and the EM1 reservoir corresponds with zones of primitive mantle preserved and protected within the subcontinental lithosphere. Lending support for their interpretation that the HIMU reservoir is metasomatized SCLM, many sub-continental mantle xenoliths plot on or near the LoNd array. Additionally, radiogenic Nd and Sr for SCLM xenoliths agree well with Nd and Sr in OIB (Othman et al., 1989; Plank and Langmuir, 1998 making it hard to distinguish SCLM vs recycled crust in OIB with radiogenic isotopes alone. Age corrected (to 230 Ma) CNE samples plot on or near the LoNd array of Hart and Zindler (1986), as do rocks from the New England Seamounts and the Azores Islands, which are all in the Atlantic at a similar latitude (~40 degrees) to the CNE magmatic province.

In regard to the HIMU signature of CNE lavas, Homrighausen et al. (2018) lend weight to theory that metasomatized SCLM is the source of the HIMU isotopic endmember. Their interpretation of the HIMU reservoir's origin is as follows: 1) Archean cratonic SCLM was metasomatized by carbonate-rich fluids and melts delivered during shallow subduction 2) Carbonate-metasomatized SCLM delaminated to the base of the mantle via 'drip tectonics' 3) Beginning in the Proterozoic, the onset of modern subduction

of oceanic crust helped initiate mantle plume activity by creating thermal boundary layers in the mantle 4) Mantle plumes today sample both Archean delaminated SCLM (HIMU) and more recent hydrothermally altered oceanic crust (FOZO: FOcal ZOne of oceanic volcanic rock arrays on isotope diagrams). They also show that HIMU volcanism is not restricted to rare occurrences as previously thought, but is instead globally distributed in oceanic intraplate, continental intraplate, and continental rift environments. Since the CNE magmatic province represents both continental intraplate melting and continental rift melting, the involvement of a HIMU component in the CNE isotopic signature seems quite plausible, however, the provenance of the HIMU-like reservoir associated with CNE volcanism is still uncertain. If the HIMU component is metasomatized SCLM, both rift-related decompression melting of in situ SCLM, or ascent of Archean-age SCLM from the deep mantle, are reasonable explanations for CNE's HIMU flavor. The latter scenario would still necessitate the involvement of a mantle plume to deliver HIMU-flavored SCLM, and since CNE trace elements and other data also support similarity to other OIB, this study still favors the plume hypothesis. Regardless of whether shallow, extant SCLM or deep, plume-carried SCLM provided the HIMU signature to CNE, neither scenario would mandate the involvement of recycled oceanic crust to explain HIMU in CNE.

The source of CNE melts appears to be relatively consistent in terms of a mixture between HIMU, EM1 and DMM (Figs. 10a-d). Summarizing the above discussion and based on the data from this study, CNE magmatism appears to be best interpreted as melting of a continuously rising (at least ~50 m.y. duration) mantle plume which contained ancient SCLM material that melted to contribute the HIMU component to CNE. In addition to SCLM, the plume also contained a portion of ancient lower crust material, which contributed the EM1 component. An alternative scenario for the presence of lower crust in the source of CNE is that Pangea's post-orogenic lower crust may have been unstable and as the mantle plume rose and began impinging on the lithosphere, it caused detachment and foundering of portions of the lower crust to become incorporated into the mantle plume's zone of melting.

#### **Potential for crustal contamination of CNE samples**

Crustal contamination of CNE magmas during ascent is unlikely or rare, as is influence of subduction-derived fluids on the source of CNE. CNE dike samples plot within, and in the OIB portion of the “mantle array” on a Pearce discrimination diagram of Nb/Yb vs Th/Yb (Fig. 5) (Pearce, 2008). This diagram compares Nb to Th because Nb is relatively enriched in OIB and MORB mantle relative to the crust, whereas Th is relatively enriched in continental crust and subduction zone magmas. Samples are normalized to Yb to minimize melt/crystallization process induced differentiation. Contrasting CNE, CAMP samples are located well above and outside the “mantle array”, indicating a much higher concentration of Th for a given Nb concentration in the source of CAMP than that of CNE. This has been interpreted as evidence for substantial mantle enrichment by subduction-derived fluids in the source for CAMP melts (Puffer, 2001; Puffer, 2003; Whalen et al., 2015).

### **Investigating evolution of CNE dike compositions due to crystallization and removal during ascent**

In order to investigate the conditions during emplacement and crystallization of the CNE dikes, major element concentration evolution during fractional crystallization of three different starting primary magma compositions was modeled with Petrolog 3.1.1.3 (Fig. 11a-b) (Danyushevsky and Plechov, 2011). Petrolog 3 is an application that can be used to model batch fractional crystallization of a given primary magma composition at specified pressures. Starting with a primary magma melt composition, Petrolog 3 evolves the composition of the liquid melt in a series of steps by modeling the crystallization of solid phases due to heat loss at a user-specified pressure. With each step, Petrolog 3 removes the crystallized solid phases and modifies the liquid melt composition accordingly. The composition of the melt at each step in the model can then be plotted on a bivariate graph of the concentration of one element versus another (MgO vs. Al<sub>2</sub>O<sub>3</sub>, for example). The resulting graph shows a “liquid line of descent” (LLD) starting from the primary magma composition. The modeled LLD can then be compared to real data to determine how well the model parameters may match up with the real conditions experienced during crystallization of a suite of magmatic samples. modeled LLDs that pass through real volcanic whole rock

data may indicate that the parameters of the model, such as depth of crystallization, starting primary magma composition, and oxygen fugacity are similar to the conditions experienced by the samples during actual fractional crystallization during/after ascent and dike emplacement.

To begin modeling the conditions of fractional crystallization and emplacement for CNE dikes, appropriate initial primary magma compositions were chosen based both on general plausibility and similarity to the compositions known in tectonic environments that match the hypotheses being tested. To test whether CNE magmatism was produced by shallow mantle melting vs. deeper mantle melting, primary magma compositions were selected from the literature for to represent mid-ocean ridge basalts (MORB) and mantle plume-associated ocean island basalts (OIB). The MORB primary magma composition is relatively depleted in incompatible trace elements due to previous melting and extraction. The OIB primary magmas are, conversely, relatively enriched in incompatible trace elements due to the incorporation of trace-element enriched recycled crust in OIB melt sources (Sun and McDonough, 1989; A W Hofmann, 1997).

The specific MORB primary magma used here was taken from Kinzler and Grove (1992) and was calculated using MORB samples from the Atlantic mid-ocean ridge. The two OIB primary magmas used here were taken from (Herzberg and Gazel, 2009) and they were calculated using OIB samples from the Azores and Hawaii, respectively. The Azores primary magma composition was chosen because the Azores hotspot is one of the geographically closest mantle-plume associated sources of OIB to the CNE magmatic province. The Azores are located in the Atlantic at a similar latitude to southeast Maine. The Hawaiian primary magma composition was chosen because the Hawaii hotspot is one of the most prolifically studied OIB locales in the world, so abundant data is available, and previous studies have identified a strong recycled crust component in the source of Hawaiian OIB, which differentiates it from the Azores OIB.

All modeled LLD produced for this study shared certain static parameters as follows: The crystallizing solid phases were olivine (ol), plagioclase (plg), and clinopyroxene (cpx), and the mineral-

melt models for these phases are taken from Danyushevsky (2001). Cotectic crystallization modeling assumed 100% fractionation for ol, plg, and cpx in equilibrium with the liquid melt (L + ol + plg + cpx). Fe<sub>2</sub>O<sub>3</sub> concentrations were calculated using QFM oxygen fugacity [f(O<sub>2</sub>)]. The f(O<sub>2</sub>) model used is from Borisov and Shapkin, 1990. Melt density was calculated using Lange and Carmichael, 1987, while melt viscosity was calculated using Bottinga and Weill, 1972.

After testing over a wide range of pressures and initial water concentrations for LLD that fall within the range of compositions of the measured CNE dike data, primary magma composition and pressure were identified as the main controls on the path of each modeled LLD. While water content of the primary magma normally exerts some control over the LLD paths, the magnitude of this effect was only apparent within a narrower set of pressures than those which were needed to encompass the CNE dike data. Different water concentrations for the primary magma compositions were checked, up to full H<sub>2</sub>O saturation, but were found not to exert as much control on the modeled LLD over the chosen pressure ranges relative to pressure and starting composition. As a result, H<sub>2</sub>O concentration was set to 0% for all modeled LLDs. However, the relative insensitivity of the LLD models to water concentration for the chosen initial primary magmas and other model parameters only serves to illustrate that it is possible the real primary magma for CNE had a concentration of H<sub>2</sub>O that was greater than 0% during fractional crystallization.

For each initial primary magma (Hawaii, Azores, and Atlantic MORB), fractional crystallization was modeled using the same set of five different pressures which ranged between 0.01 kb (shallow crystallization) and 20 kb (relatively deep crystallization). The five specific pressures modeled were 0.01 kb, 5 kb, 10 kb, 15 kb, and 20 kb. Using the standard geostatic pressure gradient of 3.7 km/kb, these approximately correspond to depths of 0 km (at or near the surface), 18.5 km, 37 km, 55.5 km, and 74 km). A separate LLD was modeled for each initial primary magma at each pressure and the results were then plotted over the measured CNE dike data (orange, blue, and green columns in Figs. 11a-b).

Broadly speaking to those results, all the LLD formed by fractional crystallization modeling of the depleted MORB-mantle primary magma matched the measured CNE dike data the most poorly, indicating that, even over a wide range of crystallization pressures, the primary magma of the CNE melting event was not sourced from the depleted MORB-mantle. The geological implication of this result is that continental rift-induced melting is not the likely melt-production mechanism for CNE magmatism. This is because continental rifting would lead to melting of the depleted upper mantle, similar to the mantle melting at mid-ocean ridges.

Still in broad terms, the Azores and Hawaiian initial primary magma compositions produced LLD that were a much better fit to the CNE dike data, relative to the Atlantic MORB primary magma. The large pressure range required to account for the CNE dike data notwithstanding, the geologic implication here is that the real primary magma for CNE magmatism was relatively enriched in incompatible trace elements

Mid-ocean ridge basalts typically crystallize at shallow depths, from 10-150 km (e.g. Langmuir and Forsyth, 2007). In contrast, ocean-island basalts crystallize at a range of depths and can experience crystallization at much greater depths than MORB, beginning at 350 km (e.g. Wyllie, 1988a; Wyllie, 1988b).

In particular, for any given MgO concentration, the LLDs for SiO<sub>2</sub> did not pass through any part of the CNE data (green column, top right of Fig. 11a). The LLD for FeO also did not pass through any part of the CNE data using a depleted MORB-mantle primary magma.

Conversely, for the Azores primary magma starting composition, SiO<sub>2</sub> and FeO LLD both matched the CNE data (blue column in Fig. 11a-b), although in the case of FeO, the range of pressures needed to pass through all CNE data was 0-20kb, or between the surface and 74 km depth. For the Azores starting primary magma, modeled LLD for TiO<sub>2</sub> and MnO were mostly too high compared to the CNE

dike data, but at the lowest pressures, the LLD did pass through a portion of the CNE dike data. Elements that fit very well for the Azores primary magma were  $\text{SiO}_2$ ,  $\text{Al}_2\text{O}_3$ , and  $\text{FeO}$ .

Lastly, the OIB starting composition from the Pacific Ocean, Hawaii's Mauna Kea produced model LLDs that most closely accounted for all CNE dike data (orange column in Fig. 11a-b), though in the case of most elements the full range of 0-20 kb pressure was needed to account for most of the CNE data. The LLD were particularly accurate during fractionation of olivine from the melt, which produces a negative slope for most of the elements when plotted against increasing MgO (Fig. 11a-b).

Due to the close fit of modeled fractional crystallization LLD derived from a primary magma composition from Mauna Kea, to real CNE dike compositions, this suggests that the source of both Mauna Kea and the CNE dikes is compositionally similar, and that, in both cases, fractional crystallization is initiating as deep as ~74 km and continuing as the magma ascends to the surface.

## **Conclusions**

The Coastal New England magmatic province consists of a suite of alkali-basalt dikes found up to 100 km inland from the coast of New England. CNE dikes can be found in Rhode Island, Massachusetts, New Hampshire, Maine, and Nova Scotia, Canada. Ages of emplacement, obtained from previous studies, mostly range from 230-200 Ma, though CNE dikes as old as 250 Ma are also known. The relatively limited variation in orientations of the CNE dikes and their correlation with structure and fabric in their host rocks, suggest that pre-existing crustal structure was a primary control on dike geometry. It is, therefore, impossible to conclusively attribute dike swarm geometry to either a radial (uplift dominated) or uniaxial (crustal rifting) event. Whole rock major element compositions in CNE basalts are higher in alkali content than basalts formed at mid-ocean ridges, with similar alkali content to that of post-shield-stage intraplate volcanism at ocean-islands that are thought to result from melting and eruption of rising mantle plume material (Fig. 3a-b).

Rare-earth element concentrations of CNE dikes, normalized to chondritic values, indicate that most CNE magmas were produced by low degrees of partial melting of a garnet-bearing source. Since garnet is stable beginning at depths of 40-80 km depending on source lithology, most CNE melts appear to have been generated at depths of at least 40-80 km or more. These depths are consistent with the results of the fractional crystallization models for CNE which suggest crystallization may have occurred as deep as ~70 km (Figs. 11a-b). A small population of CNE dikes have less fractionated MREE vs HREE than the rest of the sample set, which may reflect melts derived from a garnet-free source at shallower depths than the rest of the CNE dikes. Incompatible trace element concentrations of CNE dikes, normalized to pyrolite values, show good agreement with those of typical intraplate ocean-island magmatism, poor agreement with typical mid-ocean ridge or other shallow mantle melt sources, and moderately poor agreement with values typical for lower continental crust. In particular, pyrolite normalized concentrations of Nb and Ta do not show depletions characteristic of melt derived from subduction zone magmas or melting of the continental crust. The incompatible trace element evidence indicates that the melt source and melting conditions for CNE dikes is very similar to intraplate ocean-island basalts.

In general, radiogenic isotope ratios for CNE dikes fall on or close to the aggregate fields formed by data from intraplate ocean-island basalts (Figs. 7-9). Furthermore, CNE dikes data can be reproduced in most bivariate plots of radiogenic isotopes by mixing between recognized mantle isotope reservoirs HIMU and EMI. This is true of Sr vs eNd, Sr vs  $^{206}\text{Pb}$ , and eNd vs eHf, but CNE dike isotopic compositions cannot be produced by simple mixing of HIMU and EMI in  $^{207}\text{Pb}$  vs eNd space. This may be due to preferential enrichment of  $^{207}\text{Pb}$  in the overriding mantle or host-rock by fluxing with Pb-bearing hydrothermal fluids, and I speculate that such enrichment could have occurred by syn-subduction dehydration during the formation of Pangea. Despite preferential enrichment of  $^{207}\text{Pb}$  in continental crust relative to the mantle (Asmerom and Jacobsen, 1992), crustal contamination via assimilation is an unlikely source of  $^{207}\text{Pb}$  enrichment, because plots of crust-enriched Th and mantle-enriched Nb (Fig. 5) show that most of the CNE dike samples from this study, and in previous literature, do not plot above the

array of normal mantle-derived melt values. This indicates that contamination by melt assimilation of the crust during ascent is unlikely. Melts associated with subduction zone volcanism and crustal melting typically plot well above, and to the left, of the array formed by MORB-OIB data, indicating they are relatively enriched in Th and/or depleted in Nb (Pearce, 2008).

Aside from a small group of outliers (N = 8), incompatible trace element concentration ratios of CNE dikes from this study appear to increase as the magma evolves through crystallization, as exemplified by a plot of Mg# vs Sm/Yb (Fig. 4). This implies that fractional crystallization is an important control on incompatible element concentrations of the CNE dikes during emplacement and that the dikes have a common source. Modeling of the crystallization conditions of CNE dikes indicates that a primary melt similar to one inferred for samples from Mauna Kea, Hawaii reproduces CNE dike data far better than primary melts associated with typical mid-ocean ridge spreading centers. A relatively large range of pressures (0-20 kb) were required for crystallization-paths to reproduce as much of the CNE dike data as possible. This indicates that some CNE dikes likely experienced initial crystallization at depths up to ~70 km, while others didn't begin crystallizing until they were near the surface. Thus, although all CNE dikes apparently, they shared a common melt source, melt ascent through the lithosphere was inhibited in some cases, leading to relatively deep crystallization. The reason for this is currently unresolved, but melt ascent pathways through this relatively thick crust which contained significant pre-existing structure were clearly complex and heterogenous.

Taken together, major and trace element compositions and radiogenic isotope ratios of CNE dikes are consistent with genesis in a mantle-plume, similar to that hypothesized for modern ocean-islands such as Hawaii, the Azores or Galapagos. Dike compositions are inconsistent with melts generated at typical spreading-center ridges (i.e. MORB). The source of these melts appears to be relatively consistent in terms of a mixture between HIMU, EMI and DMM, implying involvement of at least one reservoir that retained relict subducted oceanic crust (or other similarly evolved material). The depth of melt extraction is difficult to quantify and may have been heterogenous, with some dikes implying a lack of garnet

residuum in the melt source (i.e. relatively shallow melting), while modeling suggests that the initial crystallization of some melts may have begun as deep as 70 km.

### **Future work**

Future studies of the CNE magmatic province should endeavor to collect a larger set of samples representing the entire magmatic province. One of the highest priorities should be obtaining precise ages for as many CNE dikes as possible. Many previous studies, as well as the current study, do not present ages for the dikes sampled. Dikes sampled in future studies should be age-dated to confirm that they fall within the 250-200 Ma range of ages currently associated with the CNE melting event. Specifically, the  $^{39}\text{Ar}/^{40}\text{Ar}$  age-dating technique, which utilizes stepwise heating of whole rock or mineral separates to release Ar in stages, would also provide valuable information about the cooling history of CNE melts and any subsequent reheating. A larger pool of precise ages for CNE dikes will also demonstrate whether there are any geochemical spatiotemporal trends in CNE eruptions, which would shed light on the tectonic events which led to CNE melting. Another focus for future studies would be to obtain more data on radiogenic isotope compositions of CNE dikes from across the magmatic province. Spatial trends in radiogenic isotope concentrations are found in several modern mantle-plume associated ocean-islands today, especially in Hawaii (DePaolo et al., 2001) and Galapagos (Hoernle et al, 2000). Identifying temporal and spatial trends with increased resolution would greatly benefit understanding of the CNE event.

## References

- Anderson, D. L. (1982), Hotspots, polar wander, Mesozoic convection and the geoid, *Nature*, 297(5865), 391.
- Asmerom, Y., and S. B. Jacobsen (1993), The Pb isotopic evolution of the Earth: inferences from river water suspended loads, *Earth and Planetary Science Letters*, 115(1-4), 245-256.
- Bellini, F., D. Corkum, and A. Stewart (1982), Geology of foundation excavations at Seabrook Station, Seabrook, New Hampshire, in *Geotechnology in Massachusetts*, edited.
- Beniest, A., A. Koptev, and E. Burov (2017), Numerical models for continental break-up: Implications for the South Atlantic, *Earth and Planetary Science Letters*, 461, 176-189.
- Bizimis, M., V. J. Salters, M. O. Garcia, and M. D. Norman (2013), The composition and distribution of the rejuvenated component across the Hawaiian plume: Hf-Nd-Sr-Pb isotope systematics of Kaula lavas and pyroxenite xenoliths, *Geochemistry, Geophysics, Geosystems*, 14(10), 4458-4478.
- Blackburn, T. J., P. E. Olsen, S. A. Bowring, N. M. McLean, D. V. Kent, J. Puffer, G. McHone, E. T. Rasbury, and M. Et-Touhami (2013), Zircon U-Pb geochronology links the end-Triassic extinction with the Central Atlantic Magmatic Province, *Science*, 340(6135), 941-945.
- Blichert-Toft, J., and F. Albarède (1997), The Lu-Hf isotope geochemistry of chondrites and the evolution of the mantle-crust system, *Earth and Planetary Science Letters*, 148(1-2), 243-258.
- Bohrson, W. A., and M. R. Reid (1995), Petrogenesis of alkaline basalts from Socorro Island, Mexico: Trace element evidence for contamination of ocean island basalt in the shallow ocean crust, *Journal of Geophysical Research: Solid Earth*, 100(B12), 24555-24576.
- Borisov, A., and A. Shapkin (1990), A new empirical equation rating Fe<sup>3+</sup>/Fe<sup>2+</sup> in magmas to their composition, oxygen fugacity, and temperature, *Geochem. Int.*, 27(1), 111-116.
- Bottinga, Y., and D. F. Weill (1972), The viscosity of magmatic silicate liquids; a model calculation, *American journal of science*, 272(5), 438-475.
- Boutilier, R., and C. Keen (1994), Geodynamic models of fault-controlled extension, *Tectonics*, 13(2), 439-454.
- Chadwick Jr, W., and J. Dieterich (1995), Mechanical modeling of circumferential and radial dike intrusion on Galapagos volcanoes, *Journal of Volcanology and Geothermal Research*, 66(1-4), 37-52.
- Condie, K. C. (1998), Episodic continental growth and supercontinents: a mantle avalanche connection?, *Earth and Planetary Science Letters*, 163(1-4), 97-108.
- Courtillot, V., C. Jaupart, I. Manighetti, P. Tapponnier, and J. Besse (1999), On causal links between flood basalts and continental breakup, *Earth and Planetary Science Letters*, 166(3-4), 177-195.
- Courtillot, V. E., and P. R. Renne (2003), On the ages of flood basalt events, *Comptes Rendus Geoscience*, 335(1), 113-140.
- Danyushevsky, L. V. (2001), The effect of small amounts of H<sub>2</sub>O on crystallisation of mid-ocean ridge and backarc basin magmas, *Journal of Volcanology and Geothermal Research*, 110(3-4), 265-280.

Danyushevsky, L. V., and P. Plechov (2011), Petrolog3: Integrated software for modeling crystallization processes, *Geochemistry, Geophysics, Geosystems*, 12(7).

de Lamotte, D. F., B. Fourdan, S. Leleu, F. Leparmentier, and P. de Clarens (2015), Style of rifting and the stages of Pangea breakup, *Tectonics*, 34(5), 1009-1029.

DePaolo, D. J., J. G. Bryce, A. Dodson, D. L. Shuster, and B. M. Kennedy (2001), Isotopic evolution of Mauna Loa and the chemical structure of the Hawaiian plume, *Geochemistry, Geophysics, Geosystems*, 2(7).

Dorais, M. J., M. Harper, S. Larson, H. Nugroho, P. Richardson, and N. Roosmawati (2005), A comparison of Eastern North America and Coastal New England magma suites: implications for subcontinental mantle evolution and the broad-terrane hypothesis, *Canadian Journal of Earth Sciences*, 42(9), 1571-1587.

Dye, C. J. (1986), Age, Petrology, and Structure of the Onway Dike: A Tholeiitic Pluton in Rockingham County, Southeastern New Hampshire, University of Southern Mississippi.

Eby, G. N. (1985), Sr and Pb isotopes, U and Th chemistry of the alkaline Montereian and White Mountain igneous provinces, eastern North America, *Geochimica et Cosmochimica Acta*, 49(5), 1143-1153.

Ernst, R., E. Grosfils, and D. Mege (2001), Giant dike swarms: Earth, venus, and mars, *Annual Review of Earth and Planetary Sciences*, 29(1), 489-534.

Gazel, E., T. Plank, D. W. Forsyth, C. Bendersky, C. T. A. Lee, and E. H. Hauri (2012), Lithosphere versus asthenosphere mantle sources at the Big Pine Volcanic Field, California, *Geochemistry, Geophysics, Geosystems*, 13(6).

Gudmundsson, Ó., and M. Sambridge (1998), A regionalized upper mantle (RUM) seismic model, *Journal of Geophysical Research: Solid Earth*, 103(B4), 7121-7136.

Haff, J. C. (1939), Multiple Dikes of Cape Neddick, *Bulletin of the Geological Society of America*, 50(4), 465-514.

Haff, J. C. (1941), Contaminated Complex Dike at Cape Neddick, Maine, *The Journal of Geology*, 49(8), 835-853.

Haff, J. C. (1943), Alkaline vitrophyre dike, Cape Neddick, Maine, *American Mineralogist: Journal of Earth and Planetary Materials*, 28(7-8), 426-436.

Hames, W., J. G. McHone, P. Renne, and C. Ruppel (2003), The Central Atlantic magmatic province: Insights from fragments of Pangea, Washington DC American Geophysical Union Geophysical Monograph Series, 136.

Hart, S. R., and A. Zindler (1986), In search of a bulk-Earth composition, *Chemical Geology*, 57(3-4), 247-267.

Hatcher, R. D. (2002), Alleghanian (Appalachian) orogeny, a product of zipper tectonics: Rotational transpressive continent-continent collision and closing of ancient oceans along irregular margins, *Special Paper-Geological Society of America*(364), 199-208.

- Hermes, O. D., J. Rao, M. Dickenson, and T. Pierce (1984), A transitional alkalic dolerite dike suite of Mesozoic age in southeastern New England, *Contributions to Mineralogy and Petrology*, 86(4), 386-397.
- Herzberg, C., and E. Gazel (2009), Petrological evidence for secular cooling in mantle plumes, *Nature*, 458(7238), 619.
- Hineline, M. (1988), Charles Thomas Jackson and the first geological survey of Maine, 1836–1838, *Studies in Maine geology*, 1, 1-16.
- Hirschmann, M. M., and E. M. Stolper (1996), A possible role for garnet pyroxenite in the origin of the “garnet signature” in MORB, *Contributions to Mineralogy and Petrology*, 124(2), 185-208.
- Hitchcock, C. (1861), General report upon the geology of Maine, Sixth Annual Report of the Secretary of the Maine Board of Agriculture: Augusta, Maine, Stevens and Sayward, 146-328.
- Hoal, K., B. Hoal, A. Erlank, and N. Shimizu (1994), Metasomatism of the mantle lithosphere recorded by rare earth elements in garnets, *Earth and Planetary Science Letters*, 126(4), 303-313.
- Hoernle, K., R. Werner, J. P. Morgan, D. Garbe-Schönberg, J. Bryce, and J. Mrazek (2000), Existence of complex spatial zonation in the Galápagos plume, *Geology*, 28(5), 435-438.
- Hofmann, A. (2003), Sampling mantle heterogeneity through oceanic basalts: isotopes and trace elements, *Treatise on geochemistry*, 2, 568.
- Hofmann, A. W. (1997), Mantle geochemistry: the message from oceanic volcanism, *Nature*, 385(6613), 219.
- Homrighausen, S., K. Hoernle, F. Hauff, J. Geldmacher, J.-A. Wartho, P. van den Bogaard, and D. Garbe-Schönberg (2018), Global distribution of the HIMU end member: Formation through Archean plume-lid tectonics, *Earth-science reviews*.
- Hooper, P. R. (1990), The timing of crustal extension and the eruption of continental flood basalts, *Nature*, 345(6272), 246.
- Huff, M. C. (1992), Petrography, petrology, and K-Ar geochronology of hypabyssal mafic and silicic Mesozoic igneous rocks, *Eastern North American Mesozoic Magmatism*, 268, 75.
- Hussey, A. M. (1962), The geology of southern York County, Maine, Department of Economic Development.
- Irvine, T., and W. Baragar (1971), A guide to the chemical classification of the common volcanic rocks, *Canadian journal of earth sciences*, 8(5), 523-548.
- Janney, P. E., and P. R. Castillo (2001), Geochemistry of the oldest Atlantic oceanic crust suggests mantle plume involvement in the early history of the central Atlantic Ocean, *Earth and Planetary Science Letters*, 192(3), 291-302.
- Jansa, L., and G. Pe-Piper (1985), Early Cretaceous volcanism on the northeastern American margin and implications for plate tectonics, *Geological Society of America Bulletin*, 96(1), 83-91.
- Keeley, F. (1923), Additional Notes on Igneous Rocks of Ogunquit, Maine, *Proceedings of the Academy of Natural Sciences of Philadelphia*, 105-109.

- Keeley, F. J. (1914), Notes on Some Igneous Rocks at Ogunquit, Maine, and Pigeon Cove, Mass, *Proceedings of the Academy of Natural Sciences of Philadelphia*, 3-8.
- Kelley, K. A., T. Plank, J. Ludden, and H. Staudigel (2003), Composition of altered oceanic crust at ODP Sites 801 and 1149, *Geochemistry, Geophysics, Geosystems*, 4(6).
- Kemp, J. (1890), Trap dikes near Kennebunkport, Maine: *American Geologist*, 5, 129-140.
- Khanna, T. C., M. Bizimis, G. M. Yogodzinski, and S. Mallick (2014), Hafnium–neodymium isotope systematics of the 2.7 Ga Gadwal greenstone terrane, Eastern Dharwar craton, India: implications for the evolution of the Archean depleted mantle, *Geochimica et Cosmochimica Acta*, 127, 10-24.
- Kinzler, R. J., and T. L. Grove (1992), Primary magmas of mid-ocean ridge basalts 1. Experiments and methods, *Journal of Geophysical Research: Solid Earth*, 97(B5), 6885-6906.
- Koptev, A., S. Cloetingh, E. Burov, T. François, and T. Gerya (2017), Long-distance impact of Iceland plume on Norway’s rifted margin, *Scientific reports*, 7(1), 10408.
- Lange, R. A., and I. S. Carmichael (1987), Densities of Na<sub>2</sub>O-K<sub>2</sub>O-CaO-MgO-FeO-Fe<sub>2</sub>O<sub>3</sub>-Al<sub>2</sub>O<sub>3</sub>-TiO<sub>2</sub>-SiO<sub>2</sub> liquids: new measurements and derived partial molar properties, *Geochimica et Cosmochimica Acta*, 51(11), 2931-2946.
- Langmuir, C. H., and D. W. Forsyth (2007), Mantle melting beneath mid-ocean ridges, *Oceanography*, 20(1), 78-89.
- Le Maitre, R., P. Bateman, A. Dudek, J. Keller, J. Lameyre, M. Le Bas, P. Sabine, R. Schmid, H. Sorensen, and A. Streckeisen (1989), A classification of igneous rocks and glossary of terms. Recommendations of the IUGS Subcommittee on the Systematics of Igneous rocks, London: Blackwell Scientific Publications.
- Manhes, G., C. Allegre, and A. Provost (1984), U–Th–Pb systematics of the eucrite “Juvinas”: precise age determination and evidence for exotic lead, *Geochimica et Cosmochimica Acta*, 48(11), 2247-2264.
- Manspeizer, W. (1988), Triassic–Jurassic rifting and opening of the Atlantic: an overview, in *Developments in Geotectonics*, edited, pp. 41-79, Elsevier.
- Manspeizer, W., J. H. Puffer, and H. L. Cousminer (1978), Separation of Morocco and eastern North America: a Triassic-Liassic stratigraphic record, *Geological Society of America Bulletin*, 89(6), 901-920.
- Mazza, S. E., E. Gazel, E. A. Johnson, M. J. Kunk, R. McAleer, J. A. Spotila, M. Bizimis, and D. S. Coleman (2014), Volcanoes of the passive margin: The youngest magmatic event in eastern North America, *Geology*, 42(6), 483-486.
- McDonough, W. (1991), Partial melting of subducted oceanic crust and isolation of its residual eclogitic lithology, *Philosophical Transactions of the Royal Society of London. Series A: Physical and Engineering Sciences*, 335(1638), 407-418.
- McDonough, W. F., and S.-S. Sun (1995), The composition of the Earth, *Chemical geology*, 120(3-4), 223-253.
- McHone, J. G. (1992), Mafic dike suites within Mesozoic igneous provinces of New England and Atlantic Canada, *SPECIAL PAPERS-GEOLOGICAL SOCIETY OF AMERICA*, 1-1.

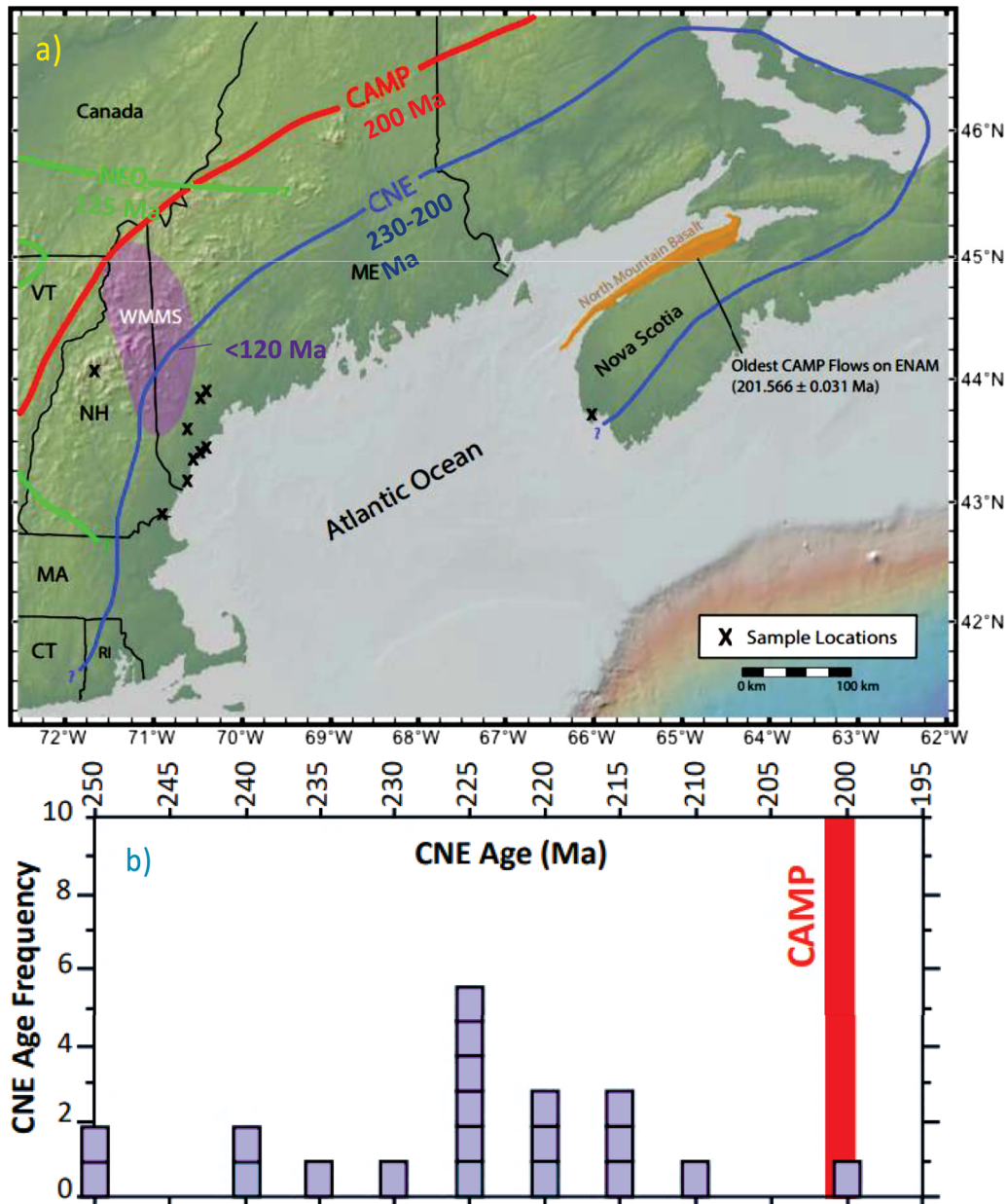
- McHone, J. G. (2000), Non-plume magmatism and rifting during the opening of the central Atlantic Ocean, *Tectonophysics*, 316(3-4), 287-296.
- McHone, J. G., and J. C. Trygstad (1982), Mesozoic mafic dikes of southern Maine, *Maine Geol*, 2, 16-32.
- McHone, J. G., and J. R. Butler (1984), Mesozoic igneous provinces of New England and the opening of the North Atlantic Ocean, *Geological Society of America Bulletin*, 95(7), 757-765.
- McHone, J. G., M. E. Ross, and J. D. Greenough (1987), Mesozoic dyke swarms of eastern North America, Mafic dyke swarms. Edited by HC Halls and WF Fahrig. Geological Association of Canada, Special Paper, 34, 279-288.
- Morency, C., M.-P. Doin, and C. Dumoulin (2002), Convective destabilization of a thickened continental lithosphere, *Earth and Planetary Science Letters*, 202(2), 303-320.
- Muller, O. H., and D. D. Pollard (1977), The stress state near Spanish Peaks, Colorado determined from a dike pattern, *Pure and Applied Geophysics*, 115(1-2), 69-86.
- Murphy, J. B., and R. D. Nance (2013), Speculations on the mechanisms for the formation and breakup of supercontinents, *Geoscience Frontiers*, 4(2), 185-194.
- Nakamura, K. (1977), Volcanoes as possible indicators of tectonic stress orientation—principle and proposal, *Journal of Volcanology and Geothermal Research*, 2(1), 1-16.
- Nance, R. D., J. B. Murphy, and M. Santosh (2014), The supercontinent cycle: a retrospective essay, *Gondwana Research*, 25(1), 4-29.
- O'Hara, M., S. Richardson, and G. Wilson (1971), Garnet-peridotite stability and occurrence in crust and mantle, *Contributions to Mineralogy and Petrology*, 32(1), 48-68.
- Odé, H. (1957), Mechanical analysis of the dike pattern of the Spanish Peaks area, Colorado, *Geological Society of America Bulletin*, 68(5), 567-576.
- Othman, D. B., W. M. White, and J. Patchett (1989), The geochemistry of marine sediments, island arc magma genesis, and crust-mantle recycling, *Earth and Planetary Science Letters*, 94(1-2), 1-21.
- Pe-Piper, G., and L. F. Jansa (1986), Triassic olivine-normative diabase from Northumberland Strait, eastern Canada: implications for continental rifting, *Canadian Journal of Earth Sciences*, 23(7), 1013-1021.
- Pe-Piper, G., and P. H. Reynolds (2000), Early Mesozoic alkaline mafic dykes, southwestern Nova Scotia, Canada, and their bearing on Triassic–Jurassic magmatism, *The Canadian Mineralogist*, 38(1), 217-232.
- Pe-Piper, G., L. F. Jansa, and R. S. J. Lambert (1992), Early Mesozoic magmatism on the eastern Canadian margin: Petrogenetic and tectonic significance, *Geological Society of America Special Papers*, 268, 13-36.
- Pearce, J. A. (2008), Geochemical fingerprinting of oceanic basalts with applications to ophiolite classification and the search for Archean oceanic crust, *Lithos*, 100(1-4), 14-48.
- Pearce, J. A., and D. W. Peate (1995), Tectonic implications of the composition of volcanic arc magmas, *Annual review of Earth and planetary sciences*, 23(1), 251-285.

- Plank, T., and C. H. Langmuir (1998), The chemical composition of subducting sediment and its consequences for the crust and mantle, *Chemical geology*, 145(3-4), 325-394.
- Puffer, J. (2001), Contrasting high field strength element contents of continental flood basalts from plume versus reactivated-arc sources, *Geology*, 29(8), 675-678.
- Puffer, J. H. (2003), A reactivated back-arc source for CAMP magma, Washington DC American Geophysical Union Geophysical Monograph Series, 136, 151-162.
- Ross, M. E., J. Puffer, and P. Ragland (1992), Petrology and tectonic significance of Mesozoic mafic dikes of the coastal New England igneous province, Massachusetts, *SPECIAL PAPERS-GEOLOGICAL SOCIETY OF AMERICA*, 63-63.
- Rudnick, R. L., and D. M. Fountain (1995), Nature and composition of the continental crust: a lower crustal perspective, *Reviews of geophysics*, 33(3), 267-309.
- Salter, V. J., S. Mallick, S. R. Hart, C. E. Langmuir, and A. Stracke (2011), Domains of depleted mantle: New evidence from hafnium and neodymium isotopes, *Geochemistry, Geophysics, Geosystems*, 12(8).
- Schlische, R. W., M. O. Withjack, and P. E. Olsen (2003), Relative timing of CAMP, rifting, continental breakup, and basin inversion: tectonic significance, *GEOPHYSICAL MONOGRAPH-AMERICAN GEOPHYSICAL UNION*, 136, 33-60.
- Sengör, A., and K. Burke (1978), Relative timing of rifting and volcanism on Earth and its tectonic implications, *Geophysical Research Letters*, 5(6), 419-421.
- Sobolev, A. V., A. W. Hofmann, D. V. Kuzmin, G. M. Yaxley, N. T. Arndt, S.-L. Chung, L. V. Danyushevsky, T. Elliott, F. A. Frey, and M. O. Garcia (2007), The amount of recycled crust in sources of mantle-derived melts, *Science*, 316(5823), 412-417.
- Steiger, R. H., and E. Jäger (1977), Subcommittee on geochronology: convention on the use of decay constants in geo- and cosmochronology, *Earth and planetary science letters*, 36(3), 359-362.
- Storey, B. C. (1995), The role of mantle plumes in continental breakup: case histories from Gondwanaland, *Nature*, 377(6547), 301.
- Sun, S.-S., and W. F. McDonough (1989), Chemical and isotopic systematics of oceanic basalts: implications for mantle composition and processes, *Geological Society, London, Special Publications*, 42(1), 313-345.
- Sundeen, D. A., and M. C. Huff (1992), Petrography, petrology, and K-Ar geochronology of hypabyssal mafic and silicic Mesozoic igneous rocks in southeastern New Hampshire, *Geological Society of America Special Papers*, 268, 75-94.
- Swanson, M. (1983), Continuous outcrop mapping within the Mesozoic eastern New England dike swarm of southern coastal Maine, paper presented at Geological Society of America Abstracts with Programs.
- Swanson, M. T. (1982), The structure and tectonics of Mesozoic dike swarms in eastern New England, State University of New York at Albany. Department of Geological Sciences.
- Swanson, M. T. (1992), Structural sequence and tectonic significance of Mesozoic dikes, *Eastern North American Mesozoic Magmatism*, 268, 37.

- Takahashi, E., and I. Kushiro (1983), Melting of a dry peridotite at high pressures and basalt magma genesis, *American Mineralogist*, 68(9-10), 859-879.
- Todt, W., R. A. Cliff, A. Hanser, and A. Hofmann (1996), Evaluation of a  $^{202}\text{Pb}$ – $^{205}\text{Pb}$  Double Spike for High-Precision Lead Isotope Analysis, *Earth processes: reading the isotopic code*, 429-437.
- Wandke, A. (1922), Intrusive rocks of the Portsmouth basin, Maine and New Hampshire, *American Journal of Science*(20), 139-158.
- Whalen, L., E. Gazel, C. Vidito, J. Puffer, M. Bizimis, W. Henika, and M. J. Caddick (2015), Supercontinental inheritance and its influence on supercontinental breakup: The Central Atlantic Magmatic Province and the breakup of Pangea, *Geochemistry, Geophysics, Geosystems*, 16(10), 3532-3554.
- White, R., and D. McKenzie (1989), Magmatism at rift zones: the generation of volcanic continental margins and flood basalts, *Journal of Geophysical Research: Solid Earth*, 94(B6), 7685-7729.
- White, W. M., F. Albarède, and P. Télouk (2000), High-precision analysis of Pb isotope ratios by multi-collector ICP-MS, *Chemical Geology*, 167(3-4), 257-270.
- Willbold, M., and A. Stracke (2006), Trace element composition of mantle end-members: Implications for recycling of oceanic and upper and lower continental crust, *Geochemistry, Geophysics, Geosystems*, 7(4).
- Wilson, J. T. (1966), Did the Atlantic close and then re-open?
- Worsley, T. R., D. Nance, and J. B. Moody (1984), Global tectonics and eustasy for the past 2 billion years, *Marine Geology*, 58(3-4), 373-400.
- Wortel, M., and S. Cloetingh (1986), On the dynamics of convergent plate boundaries and stress in the lithosphere, in *Developments in Geotectonics*, edited, pp. 115-139, Elsevier.
- Wyllie, P. J. (1988a), Magma genesis, plate tectonics, and chemical differentiation of the Earth, *Reviews of Geophysics*, 26(3), 370-404.
- Wyllie, P. J. (1988b), Solidus curves, mantle plumes, and magma generation beneath Hawaii, *Journal of Geophysical Research: Solid Earth*, 93(B5), 4171-4181.

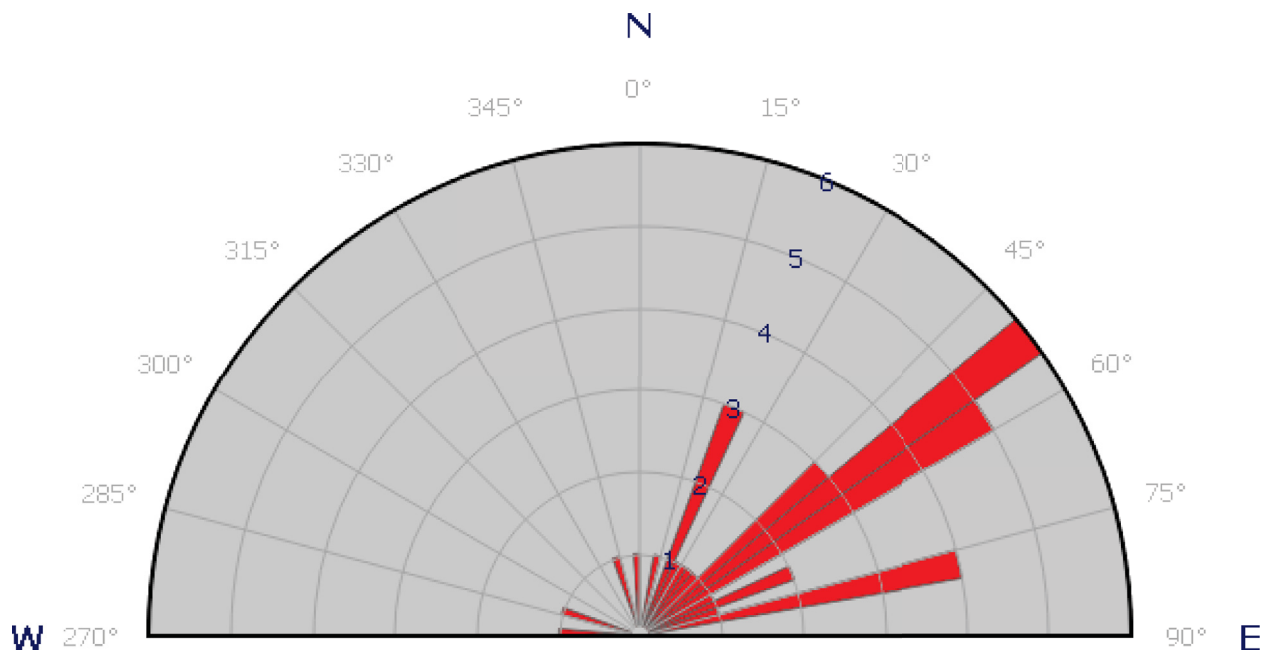
# Figures

Figure 1a-b



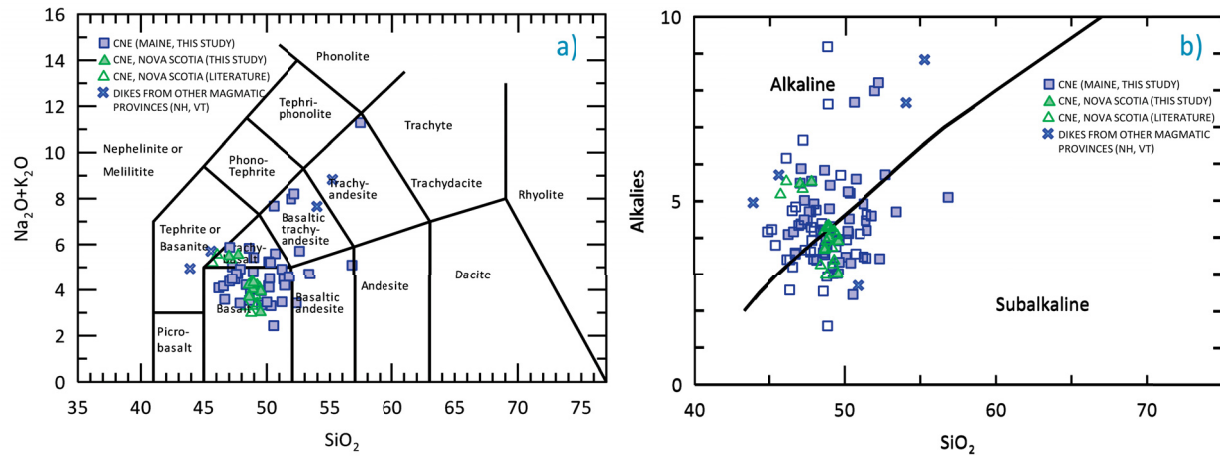
**Figure 1.** (a) Map of northeastern United States and Nova Scotia showing CNE sample dike locations (X). CNE: Coastal New England magmatic province (BLUE outline), CAMP: Central Atlantic Magmatic Province (RED outline). Adjacent, younger magmatic provinces shown for geographic reference are NEQ: New England-Quebec magmatic province (GREEN outline), WMMS: White Mountains Magmatic Suite (PURPLE shaded area). Also shown, oldest CAMP lava flows in the North Mountain Basalt (ORANGE shaded area). Magmatic province boundaries adapted from McHone and Butler (1984). (b) Histogram showing CNE sample age frequency. Most CNE samples dated to between 230-220 Ma, N=12. All CNE samples between 250-200 Ma, N=20. Age of CAMP samples shown for reference at 200 Ma. CAMP eruptions lasted only 1-2 m.y. compared to sporadic history of CNE eruptions spanning 50 m.y. Age data compiled from CNE and ENA literature (e.g. Pe-Piper and Reynolds, 2000; Dorais et al., 2005; Blackburn et al., 2013)

**Figure 2**



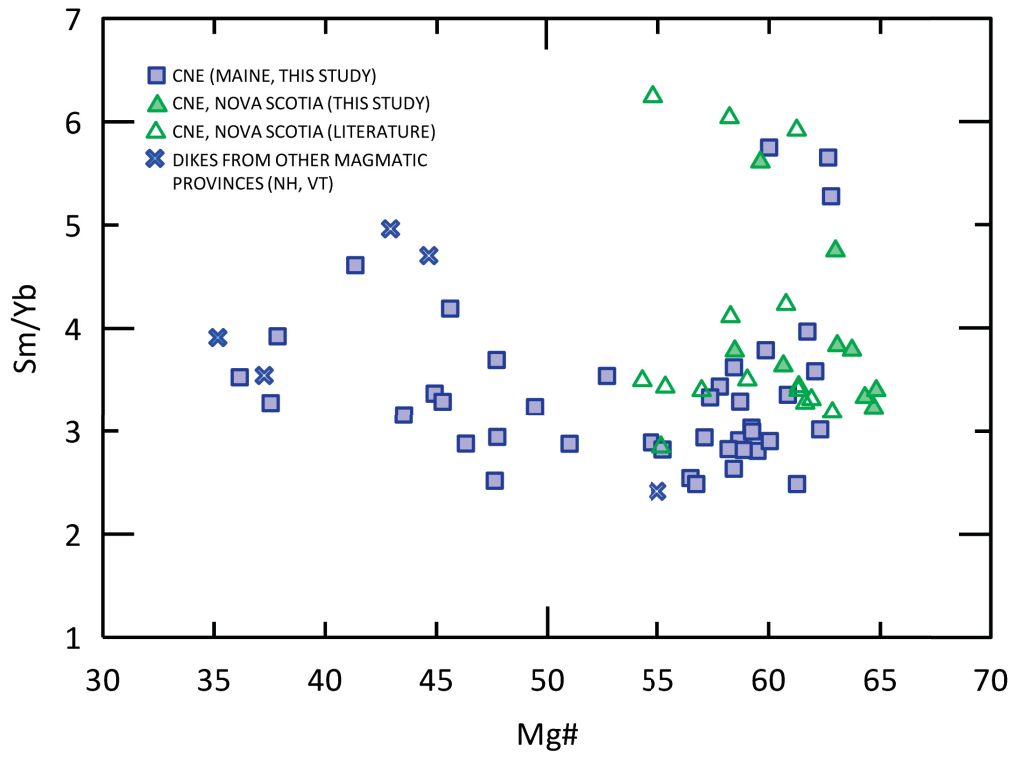
**Figure 2.** Rose diagram of CNE dike orientations (dikes in this study)

**Figure 3a-b**



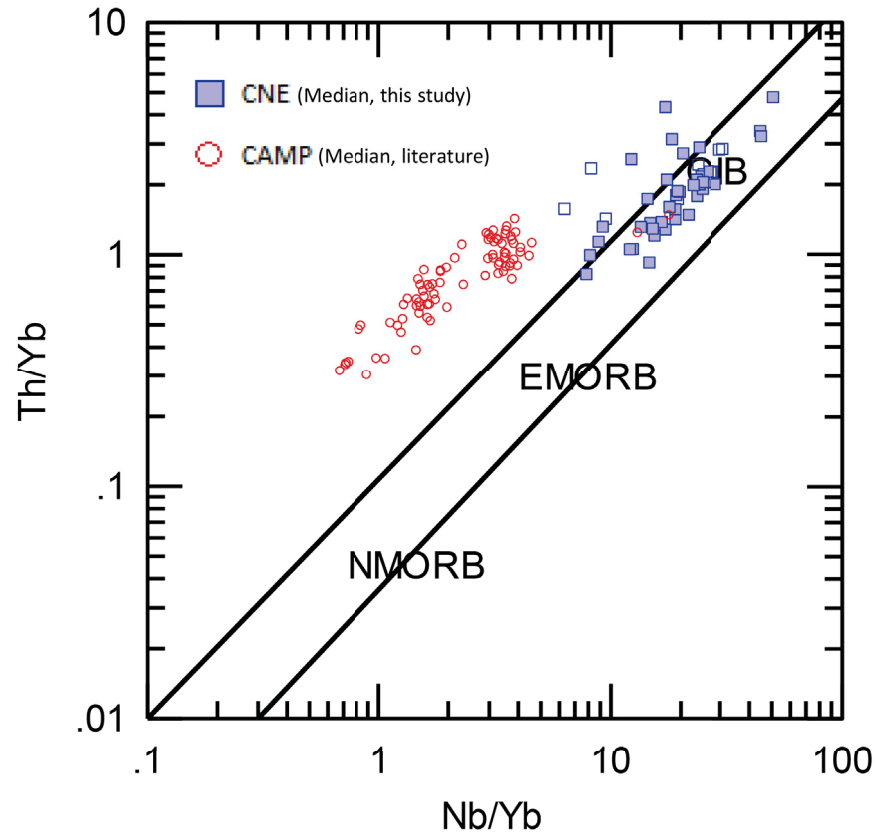
**Figure 3. (a)** Total Alkali-Silica plot (Le Maitre et al., 1989) of CNE samples (data from this study and CNE literature). **(b)** Irvine-Barager plot of alkalinity for (Irvine and Barager, 1971) for CNE samples (data from this study and CNE literature).

**Figure 4**



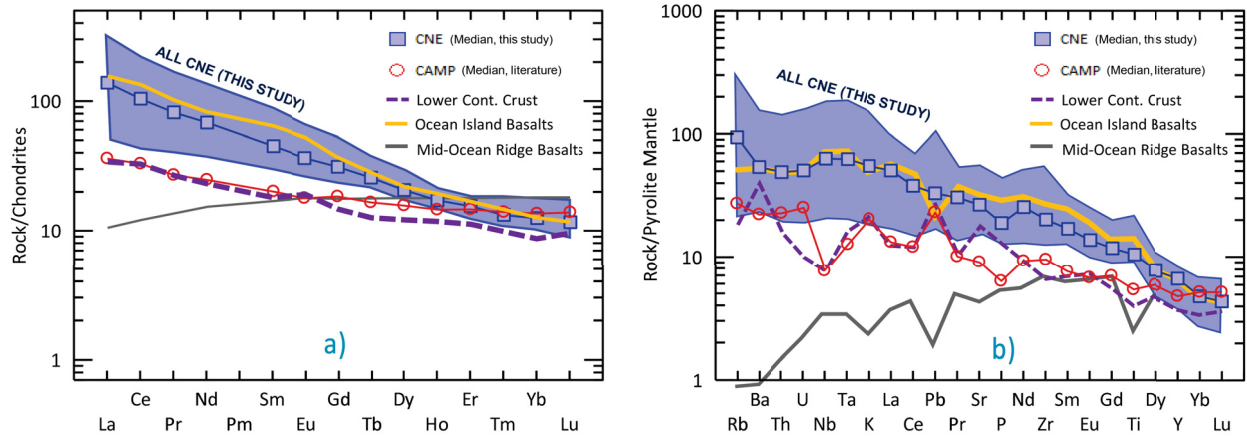
**Figure 4.** Mg#  $[(Mg/(Fe + Mg)) * 100]$  vs Sm/Yb for CNE samples (data from this study and CNE literature).

**Figure 5**



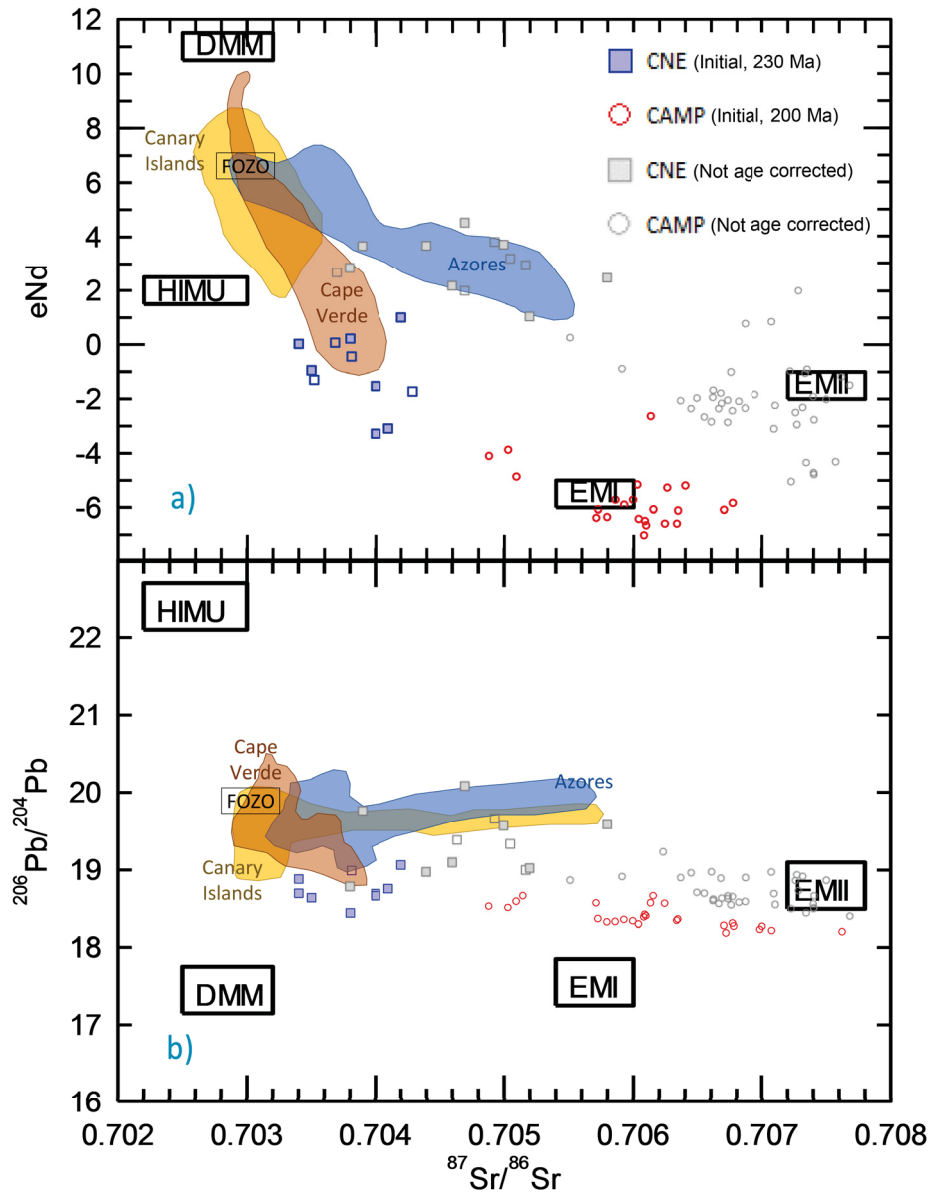
**Figure 5.** Nb/Yb vs Th/Yb (Pearce, 2008) for CNE rocks (this study + literature) and CAMP rocks. CNE samples (BLUE) overlap well with the OIB field, barring <10 outliers that plot outside the ‘array’ lines. CAMP sample (RED) plot similarly to xenoliths from the lower crust, sediments from the upper crust, and subduction-related arc volcanic samples. This diagram indicates that CNE samples are not enriched in Th relative to Nb, when normalized to Yb to account for fractionation processes such as differences in degree of partial melting. CAMP sample data from Whalen et al. (2015).

**Figure 6a-b**



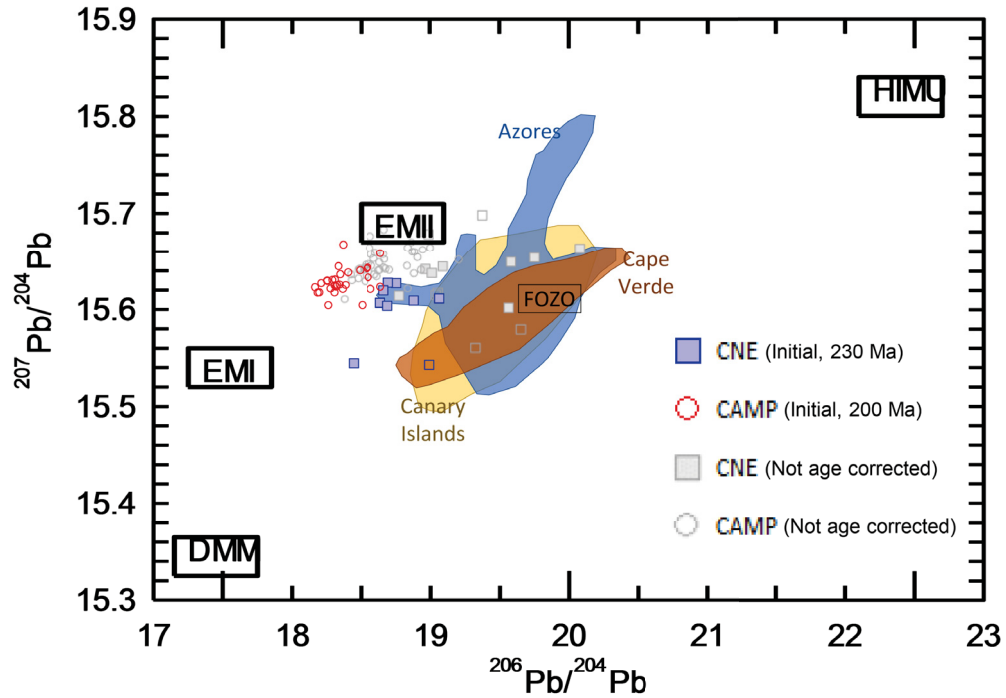
**Figure 6. (a)** Chondrite normalized spider diagram of rare-earth elements (REE) for CNE rocks (this study + literature) and CAMP rocks. CNE samples (BLUE) overlap well with typical OIB data (YELLOW). CAMP sample (RED) plot similarly to xenolith data from the Lower Continental Crust (PURPLE DASHED) for LREE, but are enriched in MREE and HREE relative to the LCC, starting at Gd through the heavier REEs. Typical MORB (GREY) included for reference. OIB, MORB, and chondrite normalization values from Sun and McDonough (1989). Lower Crust data from Rudnick and Fountain (1995). CAMP sample data from Whalen et al. (2015). **(b)** Pyrolite (primitive) mantle normalized spider diagram of incompatible trace elements for CNE rocks (this study + literature) and CAMP rocks. CNE samples (BLUE) overlap well with typical OIB data (YELLOW). CAMP samples (RED) plot similarly to xenolith data from the Lower Continental Crust (PURPLE DASHED), with the exception of Ba, U, Sr, and P, which are all relatively fluid-mobile, which indicates the involvement of subduction fluid metasomatization. Typical MORB (GREY) included for reference. OIB and MORB data from Sun and McDonough (1989). Pyrolite mantle normalization values from McDonough and Sun (1995). Lower Crust data from Rudnick and Fountain (1995). CAMP sample data from Whalen et al. (2015).

Figure 7a-b



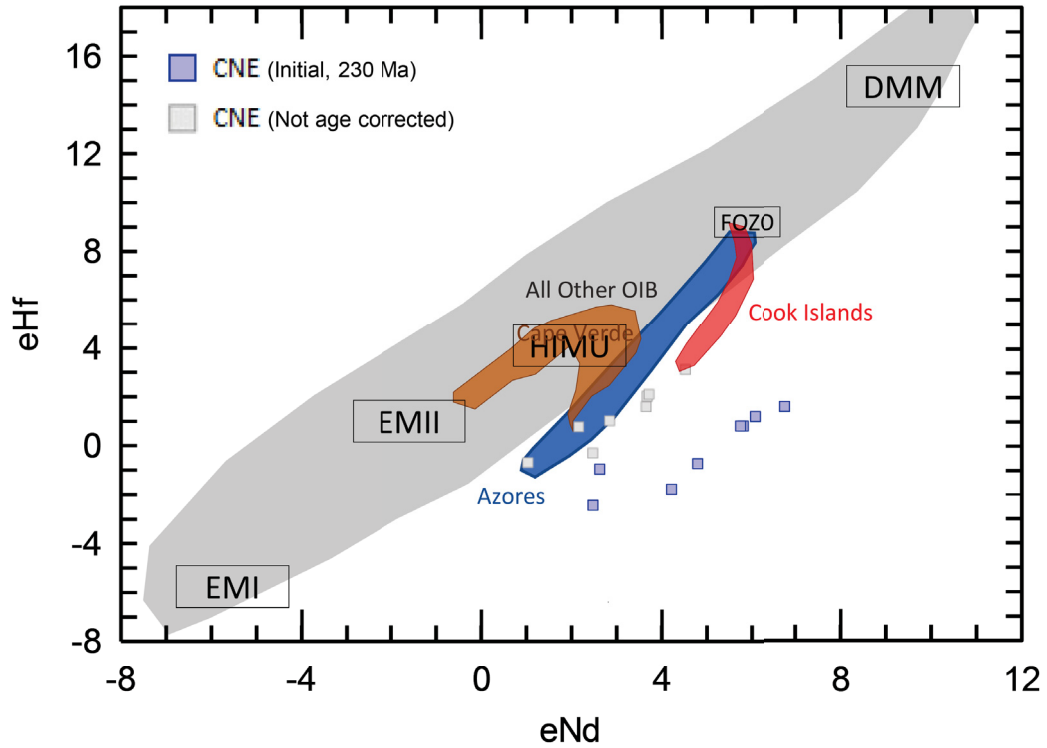
**Figure 7. (a)**  $^{87}\text{Sr}/^{86}\text{Sr}$  vs  $\text{eNd}$  for CNE rocks (this study + literature) and CAMP rocks. Age corrected CNE samples (SQUARE) and CAMP samples (CIRCLE) plotted against fields for three North Atlantic ocean island groups: Canary Islands (YELLOW FIELD), Cape Verde Islands (ORANGE FIELD), Azores Islands (BLUE FIELD). Blue squares represent initial isotopic values for CNE, age-corrected to 230 Ma. Red circles represent initial isotopic values for CAMP, age-corrected to 200 Ma. Grey squares and circles are measured isotopic values for CNE and CAMP respectively. CAMP sample data from Whalen et al. (2015). Data used for Canary Islands, Cape Verde Islands, and Azores Islands fields retrieved July 2018 from Georoc (<http://georoc.mpch-mainz.gwdg.de/georoc/>). **(b)**  $^{87}\text{Sr}/^{86}\text{Sr}$  vs  $^{206}\text{Pb}/^{204}\text{Pb}$  for CNE rocks (this study + literature) and CAMP rocks. Age corrected CNE samples (SQUARE) and CAMP samples (CIRCLE) plotted against fields for three North Atlantic ocean island groups: Canary Islands (YELLOW FIELD), Cape Verde Islands (ORANGE FIELD), Azores Islands (BLUE FIELD). Blue squares represent initial isotopic values for CNE, age-corrected to 230 Ma. Red circles represent initial isotopic values for CAMP, age-corrected to 200 Ma. Grey squares and circles are measured isotopic values for CNE and CAMP respectively. CAMP sample data from Whalen et al. (2015). Data used for Canary Islands, Cape Verde Islands, and Azores Islands fields retrieved July 2018 from Georoc.

Figure 8



**Figure 8.**  $^{207}\text{Pb}/^{204}\text{Pb}$  vs  $^{206}\text{Pb}/^{204}\text{Pb}$  for CNE rocks (this study + literature) and CAMP rocks. Age corrected CNE samples (SQUARE) and CAMP samples (CIRCLE) plotted against fields for three North Atlantic ocean island groups: Canary Islands (YELLOW FIELD), Cape Verde Islands (ORANGE FIELD), Azores Islands (BLUE FIELD). Blue squares represent initial isotopic values for CNE, age-corrected to 230 Ma. Red circles represent initial isotopic values for CAMP, age-corrected to 200 Ma. Grey squares and circles are measured isotopic values for CNE and CAMP respectively. (Pb not a good fit because of Pb contamination from continental crust). CAMP sample data from Whalen et al. (2015). Data used for Canary Islands, Cape Verde Islands, and Azores Islands fields retrieved July 2018 from Georoc.

**Figure 9**



**Figure 9.**  $eNd$  vs  $eHf$  for CNE rocks (this study + literature) and CAMP rocks. Age corrected CNE samples (SQUARE) plotted against fields for ocean island groups: Azores Islands (BLUE FIELD), Cook Islands (RED FIELD), and all other OIB data (GREY FIELD). Blue squares represent initial isotopic values for CNE, age-corrected to 230 Ma. Grey squares are measured isotopic values for CNE. DMM: Depleted MORB Mantle, EM: Enriched Mantle. Data for OIB Fields from Salters et al., 2011, Mantle Source Domains from Blichert-Toft and Albaréde, 1997. Data used for Canary Islands, Cape Verde Islands, and Azores Islands fields retrieved July 2018 from Georoc.

**Figure 10a-d**

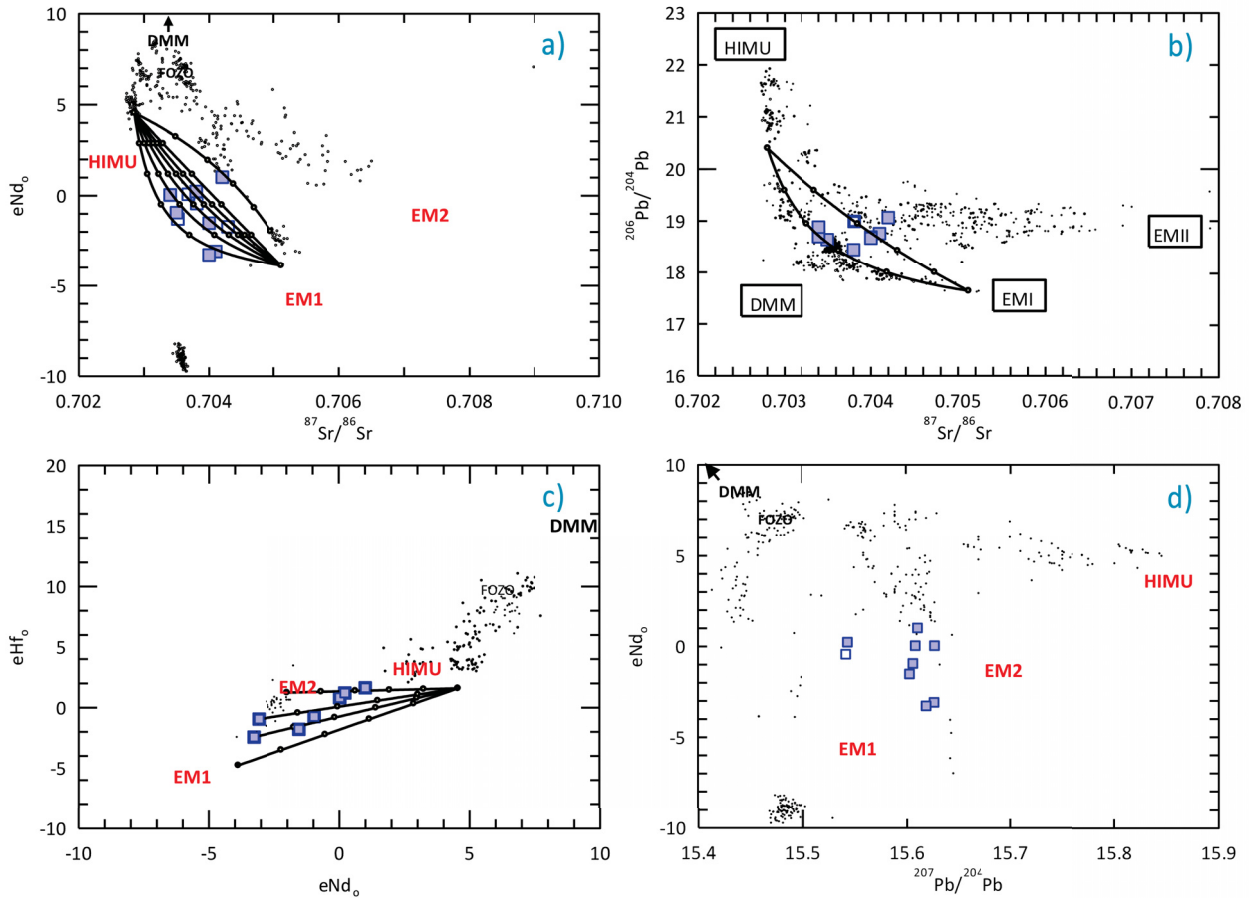


**Figure 10. (a)**  $^{87}\text{Sr}/^{86}\text{Sr}$  vs  $e\text{Nd}$  for for CNE rocks (this study + literature) and CAMP rocks. Age corrected CNE samples (SQUARE). Mixing lines between HIMU and EM1 type-localities. CAMP sample data from Whalen et al. (2015). All other data from data retrieved July 2018 from Georoc (<http://georoc.mpch-mainz.gwdg.de/georoc/>). **(b)**  $^{87}\text{Sr}/^{86}\text{Sr}$  vs  $^{206}\text{Pb}/^{204}\text{Pb}$  for CNE rocks (this study + literature) and CAMP rocks. Age corrected CNE samples (SQUARE). Mixing lines between HIMU and EM1 type-localities. CAMP sample data from Whalen et al. (2015). All other data from data retrieved July 2018 from Georoc. **(c)**  $e\text{Nd}$  vs  $e\text{Hf}$  for CNE rocks (this study + literature) and CAMP rocks. Age corrected CNE samples (SQUARE). Mixing lines between HIMU and EM1 type-localities. All other data from data retrieved July 2018 from Georoc. **(d)**  $^{207}\text{Pb}/^{204}\text{Pb}$  vs  $e\text{Nd}$  for CNE rocks (this study + literature) and CAMP rocks. Age corrected CNE samples (SQUARE). Mixing between HIMU and EM1 not conclusive. CAMP sample data from Whalen et al. (2015). All other data from data retrieved July 2018 from Georoc.

**Figure 11a**

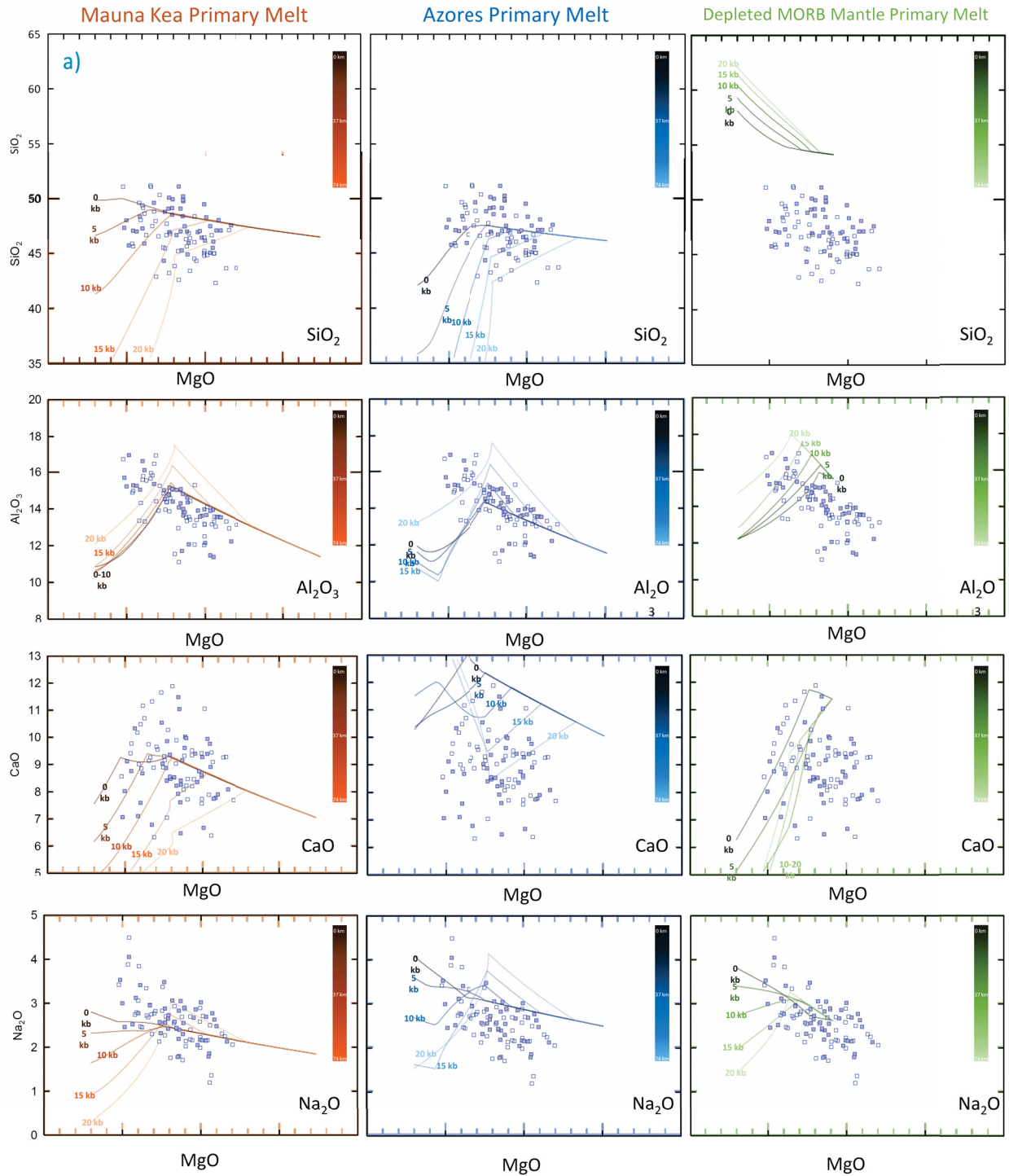


**Figure 11. (a)** MgO vs major elements with calculated liquid-lines of descent for three different starting primary magma compositions with CNE rock data (this study) for comparison. Left column is Mauna Kea primary magma composition (Herzberg and Gazel, 2009). Middle column is Azores primary magma composition (Herzberg and Gazel, 2009). Right column is MORB primary mantle composition (Kinzler and Grove, 1992).

**Figure 11b**

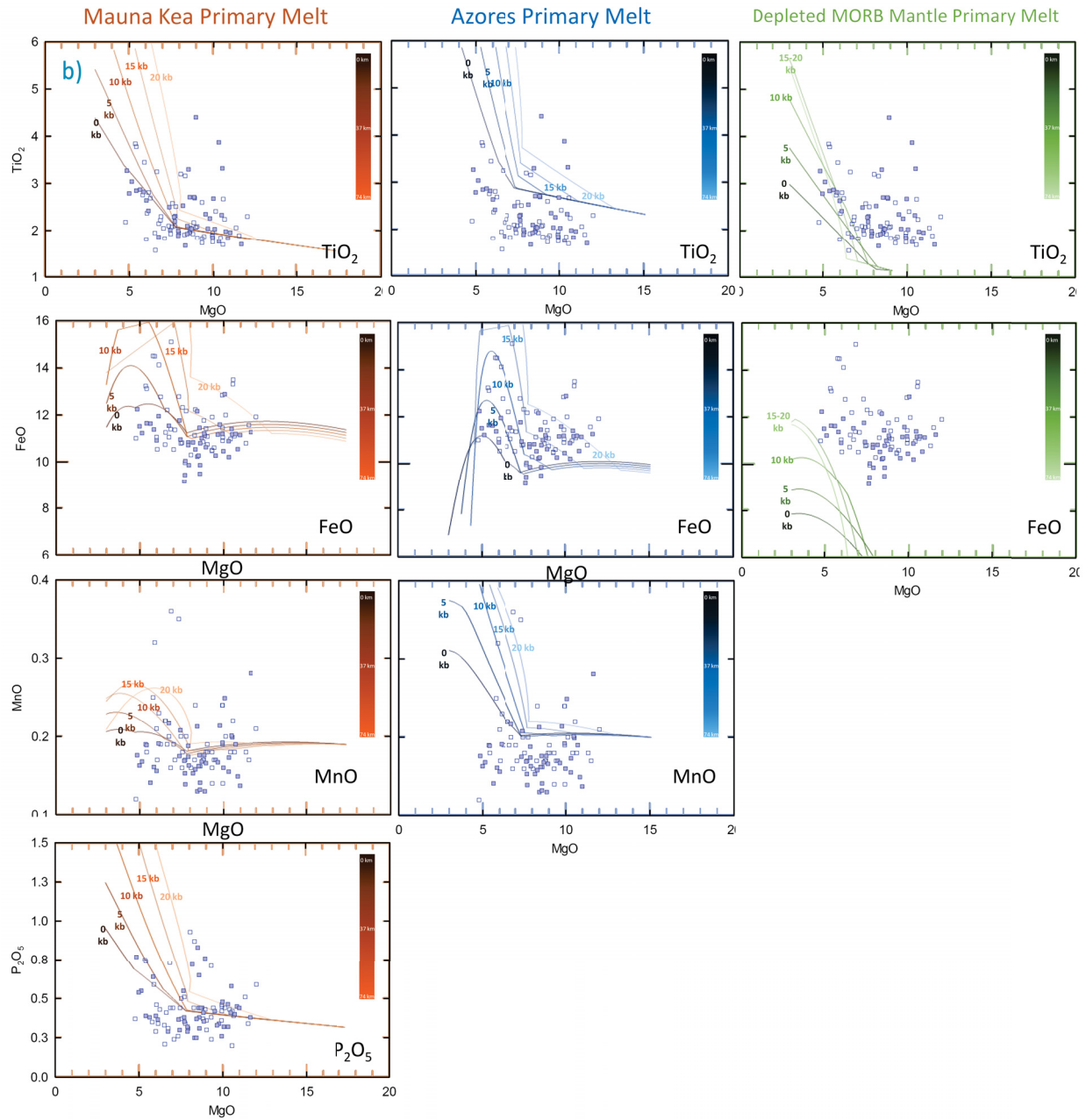


**Figure 11. (b)** MgO vs major elements with calculated liquid-lines of descent for three different starting primary magma compositions with CNE rock data (this study) for comparison. Left column is Mauna Kea primary magma composition (Herzberg and Gazel, 2009). Middle column is Azores primary magma composition (Herzberg and Gazel, 2009). Right column is MORB primary mantle composition (Kinzler and Grove, 1992).

**Table 1: Dike Locations and Orientation Data - Strike: Azimuth**

Sample	Strike	Dip	Dip Dir.	Location Name	Latitude	Longitude
<b>CNE Dike Samples from southeast Maine, USA</b>						
BC-01-6-3-2015	064	80	NW	Bald Cliff, ME	43.220683	-70.576183
BC-02-6-3-2015	075	72	NW	Bald Cliff, ME	43.220700	-70.575733
BC-03-6-3-2015	178	90	NE	Bald Cliff, ME	43.221030	-70.576100
BC-04B-6-3-2015	050	89	SE	Bald Cliff, ME	43.221200	-70.576067
BC-05-6-3-2015	049	89	NW	Bald Cliff, ME	43.221217	-70.576067
BC-06-6-3-2015	049	90	NE	Bald Cliff, ME	43.221333	-70.576000
BC-07-6-3-2015	050	90	NE	Bald Cliff, ME	43.221550	-70.576117
BC-08-6-3-2015	012	80	NW	Bald Cliff, ME	43.221567	-70.576083
BC-09-6-3-2015	059	90	NE	Bald Cliff, ME	43.221567	-70.576167
BC-10-6-3-2015	054	90	NE	Bald Cliff, ME	43.221617	-70.576417
BC-11-6-3-2015	054	90	NE	Bald Cliff, ME	43.221617	-70.576417
BC-12-6-3-2015				Bald Cliff, ME	43.221817	-70.576733
C-1-6-2-2015	120	78		Cliff Walk, ME	43.238817	-70.590367
C-2-6-2-2015	130	82		Cliff Walk, ME	43.238817	-70.590367
C-3-6-2-2015	161	90		Cliff Walk, ME	43.239450	-70.589083
C-4-6-2-2015	094	70	NE	Cliff Walk, ME	43.239450	-70.589083
C-5-6-2-2015				Cliff Walk, ME	43.241717	-70.588667
CAS-1-6-4-2015	069	78	NW	Casco, ME	43.945350	-70.549967
CAS-2-6-4-2015	058	81	NW	Casco, ME	43.945350	-70.699967
CAS-3-6-4-2015	056	90	NE	Casco, ME	43.945350	-70.549967
CAS-4-6-4-2015	065	85	NW	Casco, ME	43.945117	-70.549917
CAS-5-6-4-2015	042	80	NW	Casco, ME	43.945117	-70.549917
CAS-6-6-4-2015	058	81	NW	Casco, ME	43.945000	-70.549717
CAS-7-6-4-2015	078	90	NE	Casco, ME	43.948917	-70.526117
CAS-8-6-4-2015	058	90	NE	Casco, ME	43.948917	-70.526117
CAS-9B-6-4-2015				Casco, ME	44.000900	-70.468033
COV-1-6-3-2015	050	80	NW	Kennebunk, ME	43.343950	-70.496150
COV-2-6-3-2015	076	85	NW	Kennebunk, ME	43.343983	-70.498033
Kitt-01-6-2-2015	022	90		Kittery, ME	43.067254	-70.684361
Kitt-02-6-2-2015	024	90		Kittery, ME	43.066959	-70.684807
Kitt-03-6-2-2015	024	90		Kittery, ME	43.066324	-70.685723
Kitt-04-6-2-2015	024			Kittery, ME	43.066326	-70.685637
MIB-1-6-3-2015	052	90	NE	Wells, ME	43.301933	-70.565833
MIB-2-6-3-2015	048	65	NW	Wells, ME	43.302883	-70.565517
O-1-6-2-2015				Ogunquit, ME	43.284283	-70.571383
O-2-6-2-2015	133	65		Ogunquit, ME	43.241367	-70.600783
Port-1B-6-5-2015	120	27		Portland, ME	43.681283	-70.250867
SE-1-6-4-2015				Lake Sebago, ME	43.926967	-70.614150
Skel-1-6-5-2015	025	85	NW	Skelton Power Plant, ME	43.570617	-70.556533
Skel-2-6-5-2015	039	89	NW	Skelton Power Plant, ME	43.570667	-70.556683
Skel-3-6-5-2015	109	80	NE	Skelton Power Plant, ME	43.570900	-70.556883
Skel-4-6-5-2015	070	78	SE	Skelton Power Plant, ME	43.570883	-70.556850
Skel-5-6-5-2015	030	15	SE	Skelton Power Plant, ME	43.570700	-70.556900
Skel-6-6-5-2015	079	88	NW	Skelton Power Plant, ME	43.570467	-70.556500
<b>Dike Samples from outside CNE area for comparison</b>						
I91-150606-1				Windsor, VT	43.466620	-72.406350
LF-150606-1				Livermore Falls, NH	43.900000	-71.700000
LF-150606-3				Livermore Falls, NH	43.900000	-71.700000
Sca-150607-1				Castleton, VT	43.574140	-73.176760
<b>Nova Scotia Dike Samples from Pe-Piper and Reynolds (2000) re-analyzed for this study</b>						
78-19				Plymouth area, Nova Scotia, Canada	43.819825	-66.019474
78-27				Plymouth area, Nova Scotia, Canada	43.792778	-66.015919
78-31B				Comeau Hill, Nova Scotia, Canada	43.687689	-66.015456
78-31D				Comeau Hill, Nova Scotia, Canada	43.687689	-66.015456
78-31E				Comeau Hill, Nova Scotia, Canada	43.687689	-66.015456
78-31H				Comeau Hill, Nova Scotia, Canada	43.687689	-66.015456
78-31I				Comeau Hill, Nova Scotia, Canada	43.687689	-66.015456
78-31K				Comeau Hill, Nova Scotia, Canada	43.687689	-66.015456
78-31M				Comeau Hill, Nova Scotia, Canada	43.687689	-66.015456

**Table 2: Whole-Rock Major Element Geochemistry - Method: XRF - Units: Weight %**

Sample	SiO <sub>2</sub>	TiO <sub>2</sub>	Al <sub>2</sub> O <sub>3</sub>	FeO	CaO	MgO	MnO	K <sub>2</sub> O	Na <sub>2</sub> O	P <sub>2</sub> O <sub>5</sub>
<b>CNE Dike Samples from southeast Maine, USA</b>										
BC-01-6-3-2015	50.08	2.20	14.80	9.44	8.41	7.69	0.15	1.47	2.88	0.377
BC-02-6-3-2015	44.34	2.50	15.01	11.77	10.54	7.36	0.18	1.35	2.57	0.366
BC-03-6-3-2015	49.76	2.06	13.83	10.80	8.26	8.60	0.16	0.97	2.40	0.308
BC-04B-6-3-2015	46.93	2.31	15.15	10.04	9.86	7.71	0.14	1.32	2.56	0.352
BC-05-6-3-2015	50.85	1.96	15.61	9.92	7.16	5.06	0.15	2.26	3.25	0.293
BC-06-6-3-2015	49.48	1.85	13.97	11.19	8.61	9.93	0.19	0.21	2.17	0.263
BC-07-6-3-2015	51.95	1.73	14.94	8.73	7.71	7.12	0.13	1.98	2.59	0.368
BC-08-6-3-2015	51.10	1.67	14.07	10.54	8.23	8.31	0.16	0.76	2.58	0.254
BC-09-6-3-2015	50.20	1.98	13.64	9.86	8.41	8.59	0.14	3.02	1.80	0.384
BC-10-6-3-2015	49.08	2.29	14.74	9.15	8.87	7.65	0.17	1.60	3.48	0.550
BC-11-6-3-2015	47.00	2.10	15.07	10.23	11.48	8.43	0.13	0.93	2.42	0.367
BC-12-6-3-2015	49.93	1.95	14.39	9.86	8.48	7.92	0.16	1.34	2.73	0.309
C-1-6-2-2015	46.99	2.87	15.25	11.63	10.33	5.63	0.14	0.89	2.52	0.377
C-2-6-2-2015	46.07	3.32	11.38	11.18	8.91	10.51	0.20	3.89	1.86	0.579
C-3-6-2-2015	44.92	2.69	14.35	11.13	10.02	8.87	0.13	1.46	2.55	0.355
C-4-6-2-2015	45.51	2.33	13.94	11.41	9.76	10.47	0.20	1.70	1.79	0.408
C-5-6-2-2015	46.66	2.53	15.02	10.83	8.53	8.17	0.15	1.73	3.06	0.719
CAS-1-6-4-2015	48.36	2.82	15.04	11.38	7.11	5.84	0.16	1.94	3.12	0.642
CAS-2-6-4-2015	47.32	3.27	15.69	12.25	7.07	4.84	0.18	1.71	3.53	0.768
CAS-3-6-4-2015	48.40	1.95	14.81	11.45	7.62	8.56	0.18	1.16	2.19	0.442
CAS-4-6-4-2015	49.05	1.94	17.62	8.99	5.49	3.07	0.17	2.51	5.02	0.503
CAS-5-6-4-2015	49.13	1.89	15.05	10.83	8.55	7.89	0.19	1.60	2.42	0.322
CAS-6-6-4-2015	50.31	1.80	17.24	9.45	5.50	3.00	0.19	3.37	4.53	0.907
CAS-7-6-4-2015	60.79	0.10	20.20	3.80	0.97	0.07	0.19	4.32	8.89	0.104
CAS-8-6-4-2015	55.05	0.91	17.51	6.72	2.91	1.23	0.19	4.54	6.26	0.368
CAS-9B-6-4-2015	45.90	2.42	16.10	11.95	8.67	6.12	0.19	1.11	3.41	0.365
COV-1-6-3-2015	45.73	3.04	16.92	11.23	9.12	5.13	0.17	2.39	2.46	0.550
COV-2-6-3-2015	47.26	2.64	16.60	10.92	7.60	6.00	0.16	2.90	2.77	0.394
Kitt-01-6-2-2015	49.61	1.86	15.35	11.54	6.79	6.73	0.22	2.52	2.95	0.292
Kitt-02-6-2-2015	48.80	2.01	14.53	10.96	9.03	7.42	0.21	1.74	2.32	0.299
Kitt-03-6-2-2015	46.98	2.71	14.61	11.22	9.61	8.84	0.18	2.12	2.30	0.414
Kitt-04-6-2-2015	46.43	2.26	13.62	11.59	8.75	9.77	0.21	2.54	2.05	0.338
MIB-1-6-3-2015	47.06	2.85	15.28	11.65	8.76	5.40	0.19	0.55	4.05	0.390
MIB-2-6-3-2015	48.01	2.79	15.22	11.52	8.03	4.98	0.16	1.31	3.00	0.541
O-1-6-2-2015	51.57	1.90	16.59	9.37	5.04	2.85	0.17	3.13	4.17	0.591
O-2-6-2-2015	49.87	2.71	14.00	9.49	6.48	8.58	0.13	1.59	2.83	0.650
Port-1B-6-5-2015	55.23	2.38	16.20	8.17	5.95	3.84	0.12	0.47	4.48	0.301
SE-1-6-4-2015	48.47	2.43	17.44	9.97	5.80	3.36	0.23	2.62	4.73	0.774
Skel-1-6-5-2015	45.07	3.87	11.47	10.89	9.39	10.30	0.16	2.04	2.15	0.463
Skel-2-6-5-2015	48.53	2.00	15.07	10.72	9.36	7.89	0.17	1.22	2.65	0.286
Skel-3-6-5-2015	48.30	2.03	13.66	12.88	6.68	10.06	0.25	1.08	2.16	0.320
Skel-4-6-5-2015	46.93	2.35	13.90	10.27	9.40	9.52	0.17	1.42	2.67	0.415
Skel-5-6-5-2015	45.96	4.40	12.06	10.63	9.97	8.94	0.17	1.46	2.90	0.761
Skel-6-6-5-2015	49.09	1.93	14.30	12.16	7.93	8.42	0.21	0.78	2.44	0.254
<b>Dike Samples from outside CNE area for comparison</b>										
I91-150606-1	49.65	1.75	14.47	11.28	9.62	7.73	0.16	0.28	2.33	0.254
LF-150606-1	43.72	3.93	15.15	12.43	9.09	5.24	0.19	2.16	3.31	0.687
LF-150606-3	42.07	4.48	14.56	13.60	9.58	6.15	0.17	1.82	2.92	0.461
Sca-150607-1	53.31	1.69	17.10	7.78	4.35	2.59	0.19	2.77	5.74	0.883
<b>Nova Scotia Dike Samples from Pe-Piper and Reynolds (2000) re-analyzed for this study</b>										
78-19	45.29	3.30	11.70	10.27	11.04	8.50	0.16	3.50	1.78	0.831
78-27	46.16	2.68	12.14	10.46	9.27	9.98	0.16	2.33	3.02	0.480
78-31B	48.04	1.83	13.56	10.55	7.78	10.84	0.15	1.17	2.63	0.450
78-31D	47.03	2.04	13.57	11.17	8.36	9.65	0.17	1.00	2.86	0.328
78-31E	47.08	1.96	13.53	11.15	7.91	10.98	0.14	1.13	2.48	0.437
78-31H	47.08	1.98	13.54	11.19	7.75	10.71	0.19	1.30	2.77	0.400
78-31I	47.47	1.76	13.89	10.21	9.94	10.31	0.17	0.90	2.69	0.315
78-31K	47.46	2.04	13.81	11.01	9.16	8.69	0.17	1.12	3.05	0.444
78-31M	47.55	1.70	12.22	11.27	8.09	11.64	0.28	0.76	2.13	0.378

**Table 3: Whole-Rock Trace Element Geochemistry - Method: LA-ICP-MS - Units: PPM**

Sample	Sc	V	Cr	Co	Ni	Cu	Zn	Ga	Ge	Rb	Sr	Y
<b>CNE Dike Samples from southeast Maine, USA</b>												
BC-01-6-3-2015	29.38	187.92	224.93	40.79	129.65	37.56	114.10	21.91	1.87	32.23	458.63	31.67
BC-02-6-3-2015	27.66	213.85	239.33	44.53	110.37	61.82	124.61	19.63	1.57	56.87	492.94	24.82
BC-03-6-3-2015	29.40	186.43	297.90	46.90	212.85	71.14	129.77	21.42	1.57	19.05	345.81	25.15
BC-04B-6-3-2015	28.18	198.63	285.65	37.31	109.18	53.63	113.17	18.36	1.71	46.13	443.27	25.47
BC-05-6-3-2015	28.54	177.84	137.42	26.55	35.40	35.20	173.61	23.00	1.47	95.44	414.11	28.90
BC-06-6-3-2015	17.65	193.26	304.08	56.53	233.68	70.83	133.50	21.02	1.37	5.27	322.75	24.16
BC-07-6-3-2015	16.23	149.64	236.11	37.35	169.52	51.98	121.61	21.92	1.27	42.75	351.06	28.65
BC-08-6-3-2015	18.24	169.37	273.92	44.84	173.54	71.72	133.93	21.26	1.44	16.28	306.74	22.97
BC-09-6-3-2015	13.84	192.39	273.71	47.61	194.44	11.70	101.34	22.06	1.36	156.17	492.15	26.81
BC-10-6-3-2015	15.60	189.22	248.92	37.00	153.24	45.37	109.60	22.07	1.75	31.00	472.39	27.54
BC-11-6-3-2015	30.08	207.64	335.40	43.35	146.90	60.93	191.33	22.39	1.54	15.73	435.21	29.07
BC-12-6-3-2015	34.28	190.77	282.78	40.44	110.05	29.75	103.19	22.25	1.53	43.46	385.05	34.04
C-1-6-2-2015	26.02	229.33	59.13	42.45	46.08	78.83	171.18	25.62	1.67	32.68	565.25	34.89
C-2-6-2-2015	24.96	227.94	260.83	45.30	128.95	4.58	151.79	34.11	1.78	167.82	827.39	33.13
C-3-6-2-2015	26.98	218.28	240.19	48.71	156.44	60.62	160.11	24.40	1.75	32.63	610.10	27.15
C-4-6-2-2015	25.64	218.23	264.58	52.31	171.75	32.57	139.40	22.15	1.66	78.12	410.58	29.23
C-5-6-2-2015	30.12	163.35	211.55	39.73	172.84	51.62	129.28	22.92	1.72	40.77	792.33	34.59
CAS-1-6-4-2015	24.47	171.20	106.66	37.65	95.26	52.86	147.91	22.77	1.43	178.04	581.69	33.37
CAS-2-6-4-2015	24.94	176.08	13.26	37.43	52.05	47.04	168.89	22.50	1.62	94.76	775.23	34.83
CAS-3-6-4-2015	27.54	173.53	280.50	48.02	182.47	51.39	133.88	21.93	1.40	93.37	495.71	28.95
CAS-4-6-4-2015	19.15	73.98	1.68	16.88	7.42	8.97	85.85	29.70	1.35	56.25	760.27	26.81
CAS-5-6-4-2015	28.75	182.05	294.77	44.89	152.98	56.91	142.57	25.79	1.44	125.81	442.29	32.42
CAS-6-6-4-2015	23.12	71.41	4.83	19.21	7.82	7.25	132.53	22.87	1.53	157.98	800.98	32.53
CAS-7-6-4-2015	30.53	0.35	1.09	0.09	5.53	1.59	148.96	22.81	1.74	168.78	74.44	52.95
CAS-8-6-4-2015	24.00	7.05	0.68	4.80	-10.65	2.07	102.58	37.41	1.59	170.13	437.75	34.32
CAS-9B-6-4-2015	26.66	186.42	180.86	41.63	73.90	54.51	109.04	19.95	1.53	51.13	499.54	26.27
COV-1-6-3-2015	12.74	256.20	39.64	37.51	38.51	38.57	112.70	22.13	1.43	116.44	774.37	25.26
COV-2-6-3-2015	26.59	232.65	76.53	36.46	46.86	53.47	120.34	29.56	1.48	128.59	794.59	29.69
Kitt-01-6-2-2015	27.11	176.79	201.63	39.50	88.96	18.00	130.17	23.92	1.54	108.34	381.55	24.16
Kitt-02-6-2-2015	28.34	186.48	209.74	33.88	114.36	15.15	117.44	19.08	1.48	106.69	359.85	24.93
Kitt-03-6-2-2015	27.56	224.97	241.21	46.64	137.04	42.17	140.50	27.27	1.50	66.88	624.42	30.13
Kitt-04-6-2-2015	26.84	211.45	324.91	47.98	152.87	18.05	148.86	25.39	1.43	93.18	395.18	26.96
MIB-1-6-3-2015	27.30	262.96	81.74	37.47	38.75	58.72	129.20	23.02	1.98	16.00	526.21	35.16
MIB-2-6-3-2015	27.81	203.87	78.54	33.16	48.73	45.28	129.36	22.05	1.42	28.21	529.86	35.36
O-1-6-2-2015	24.17	77.12	6.51	18.60	-0.56	15.53	166.43	38.14	1.55	79.18	784.83	41.12
O-2-6-2-2015	27.42	178.30	164.06	47.00	131.56	44.58	120.10	21.78	1.63	43.55	277.69	31.50
Port-1B-6-5-2015	26.70	113.44	71.92	27.37	43.77	21.26	109.04	18.65	1.30	12.99	565.53	16.43
SE-1-6-4-2015	1.55	94.20	1.41	19.03	11.70	14.17	107.00	22.69	1.67	85.71	1090.27	35.66
Skel-1-6-5-2015	27.54	218.45	387.28	45.70	201.71	45.49	112.43	24.65	1.85	61.97	739.00	29.55
Skel-2-6-5-2015	27.67	222.51	306.75	42.91	91.55	44.08	114.31	22.26	1.45	51.76	412.78	31.63
Skel-3-6-5-2015	25.46	187.71	312.98	52.43	238.57	63.02	123.83	21.98	1.47	53.56	381.15	28.30
Skel-4-6-5-2015	31.17	214.92	373.90	46.12	157.29	48.81	117.31	22.42	1.47	61.08	575.64	30.89
Skel-5-6-5-2015	14.84	257.69	283.59	44.49	149.76	44.98	138.93	22.27	1.75	43.24	924.14	35.62
Skel-6-6-5-2015	27.18	196.10	316.58	47.87	167.28	62.74	127.41	22.06	1.39	26.30	342.74	28.78
<b>Dike Samples from outside CNE area for comparison</b>												
I91-150606-1	28.44	217.34	220.09	49.12	158.65	122.15	129.59	21.19	1.49	6.46	334.94	22.58
LF-150606-1	23.81	196.79	6.78	36.51	35.70	26.22	139.81	23.66	1.62	60.48	1091.69	36.42
LF-150606-3	24.06	264.64	10.61	48.23	33.06	44.44	171.48	32.25	1.96	42.96	966.35	38.46
Sca-150607-1	5.01	53.29	1.06	11.17	6.77	3.03	118.88	24.39	2.15	59.75	1283.40	37.32
<b>Nova Scotia Dike Samples from Pe-Piper and Reynolds (2000) re-analyzed for this study</b>												
78-19	11.52	235.17	268.62	49.28	108.43	52.10	154.17	23.60	1.76	119.04	924.28	30.41
78-27	25.20	209.35	339.01	56.98	203.69	48.34	133.69	30.06	1.33	109.78	877.66	24.41
78-31B	10.56	162.14	247.10	48.99	241.65	50.41	112.12	21.86	1.34	50.43	642.08	25.10
78-31D	26.99	243.15	319.79	55.05	195.33	64.62	138.72	23.61	1.49	56.38	550.69	21.43
78-31E	10.85	174.92	275.68	50.47	208.28	59.83	125.14	21.89	1.46	53.07	605.05	25.51
78-31H	10.80	193.46	268.09	51.02	219.52	60.48	154.23	22.00	1.49	62.13	611.84	23.55
78-31I	25.55	197.27	335.87	53.87	214.58	54.65	109.42	23.32	1.42	27.85	638.16	21.11
78-31K	14.44	202.92	282.63	51.13	189.11	58.72	137.71	21.86	1.46	33.76	611.15	23.26
78-31M	9.12	168.96	289.53	69.87	418.24	60.06	135.56	21.29	1.51	46.12	524.32	22.18

**Table 3 (cont.): Whole-Rock Trace Element Geochemistry - Method: LA-ICP-MS - Units: PPM**

Sample	Zr	Nb	Cs	Ba	La	Ce	Pr	Nd	Sm	Eu	Gd	Tb
<b>CNE Dike Samples from southeast Maine, USA</b>												
BC-01-6-3-2015	282.37	43.63	1.93	325.43	35.00	66.66	8.14	33.98	7.21	2.17	6.79	1.02
BC-02-6-3-2015	157.66	32.26	8.14	231.49	26.07	56.50	7.01	30.65	6.63	2.02	6.40	0.90
BC-03-6-3-2015	177.46	23.17	7.43	175.44	17.68	37.59	4.54	21.32	5.41	1.73	5.68	0.82
BC-04B-6-3-2015	194.02	39.35	1.15	180.11	29.86	62.85	7.64	31.71	6.59	2.01	5.91	0.93
BC-05-6-3-2015	211.70	26.51	0.94	348.51	26.06	54.85	6.69	28.96	6.02	1.73	6.12	1.04
BC-06-6-3-2015	130.13	15.21	2.05	87.48	13.22	25.15	3.63	16.43	4.82	1.63	5.25	0.73
BC-07-6-3-2015	310.70	35.35	0.28	345.39	38.29	70.12	8.40	34.47	6.82	1.91	6.23	0.93
BC-08-6-3-2015	132.43	13.94	3.07	138.31	12.24	23.87	3.20	14.88	4.50	1.48	4.89	0.71
BC-09-6-3-2015	220.12	36.50	4.46	442.82	37.22	69.56	8.72	33.78	7.12	1.86	6.11	0.86
BC-10-6-3-2015	261.10	48.96	0.47	436.02	42.42	75.30	9.38	37.19	7.69	2.38	6.75	1.03
BC-11-6-3-2015	199.51	33.26	1.23	289.03	28.53	53.21	6.96	28.91	6.31	1.99	6.07	0.89
BC-12-6-3-2015	291.16	31.80	2.35	257.95	36.57	63.69	8.28	34.62	7.29	1.96	7.31	1.08
C-1-6-2-2015	206.95	35.34	0.75	254.18	26.96	54.93	7.06	30.98	6.93	2.49	6.94	1.10
C-2-6-2-2015	356.97	99.35	23.51	907.46	73.26	129.05	15.56	61.41	11.08	3.35	9.39	1.27
C-3-6-2-2015	211.99	47.40	25.97	416.10	31.99	71.04	8.33	35.87	6.88	2.33	6.58	1.00
C-4-6-2-2015	209.12	37.89	11.46	216.13	30.72	59.33	7.55	30.88	7.10	2.17	6.26	0.93
C-5-6-2-2015	295.50	57.31	1.75	515.73	44.45	80.90	10.29	43.63	8.80	2.86	8.56	1.23
CAS-1-6-4-2015	317.60	48.46	11.10	356.22	36.97	69.72	9.12	41.25	9.05	2.64	8.42	1.25
CAS-2-6-4-2015	311.87	58.95	5.36	400.72	40.86	82.42	10.34	44.83	10.47	3.10	9.12	1.31
CAS-3-6-4-2015	196.63	41.91	12.61	393.19	32.96	65.82	7.42	31.89	6.34	1.92	5.93	0.86
CAS-4-6-4-2015	315.46	77.33	1.07	663.80	51.53	109.08	12.40	47.84	8.58	2.35	6.54	1.01
CAS-5-6-4-2015	251.52	41.58	13.02	425.69	35.20	64.94	7.76	30.95	6.05	2.11	6.01	0.93
CAS-6-6-4-2015	416.48	94.99	2.67	688.13	70.49	130.04	14.32	54.73	9.28	2.69	7.71	1.06
CAS-7-6-4-2015	1318.79	197.76	2.78	7.92	116.86	186.89	17.50	55.68	8.78	0.23	8.71	1.50
CAS-8-6-4-2015	591.39	119.99	2.71	1047.52	74.14	131.62	14.51	50.41	8.32	2.35	6.51	1.00
CAS-9B-6-4-2015	155.65	37.28	4.65	261.88	26.94	59.87	7.23	31.15	6.38	1.97	5.93	0.87
COV-1-6-3-2015	173.51	31.86	0.58	380.58	25.87	51.54	6.82	29.19	6.47	2.22	5.95	0.85
COV-2-6-3-2015	196.29	38.13	1.25	578.86	30.01	58.86	7.53	31.89	6.51	2.22	6.46	0.99
Kitt-01-6-2-2015	190.59	26.84	4.51	266.19	26.93	52.58	6.39	25.97	5.72	1.90	5.36	0.76
Kitt-02-6-2-2015	163.25	26.95	8.54	209.09	22.58	49.37	6.00	25.70	5.41	1.71	5.62	0.86
Kitt-03-6-2-2015	224.83	47.13	7.63	471.57	33.75	64.47	8.14	34.88	7.25	2.46	6.97	1.08
Kitt-04-6-2-2015	203.67	37.57	10.37	403.64	27.80	54.25	6.74	27.30	5.74	2.00	5.70	0.87
MIB-1-6-3-2015	233.93	36.14	0.33	160.36	32.40	64.41	8.40	34.93	7.70	2.26	7.47	1.12
MIB-2-6-3-2015	209.21	40.51	7.91	358.64	34.73	68.08	8.73	38.73	8.43	2.53	8.39	1.28
O-1-6-2-2015	442.09	74.03	5.52	933.88	69.58	130.71	15.46	59.08	11.03	3.08	9.29	1.37
O-2-6-2-2015	245.77	54.93	1.27	291.08	40.88	78.94	9.49	39.91	8.69	2.69	7.86	1.10
Port-1B-6-5-2015	122.80	11.44	0.72	152.27	9.83	24.04	3.42	18.51	5.02	1.79	4.62	0.64
SE-1-6-4-2015	393.94	88.93	1.35	744.67	64.22	118.46	14.21	55.55	9.80	3.06	8.02	1.19
Skel-1-6-5-2015	347.49	53.58	8.80	422.74	36.46	85.71	11.26	52.23	11.36	3.27	9.31	1.27
Skel-2-6-5-2015	191.84	22.75	14.96	243.38	22.67	42.88	5.64	24.76	6.11	1.83	6.22	0.92
Skel-3-6-5-2015	164.75	22.35	15.41	167.34	17.67	33.64	4.52	20.34	5.22	1.85	5.37	0.84
Skel-4-6-5-2015	220.63	42.40	13.33	339.10	33.19	61.94	7.77	33.15	7.14	2.36	6.67	1.01
Skel-5-6-5-2015	444.41	65.82	3.51	455.73	48.90	97.32	13.56	63.05	13.28	3.82	10.87	1.43
Skel-6-6-5-2015	153.32	16.67	8.65	173.90	14.91	28.50	4.12	19.18	5.30	1.60	5.74	0.86
<b>Dike Samples from outside CNE area for comparison</b>												
I91-150606-1	102.78	18.28	1.94	160.57	13.08	26.87	3.52	15.36	4.03	1.43	4.63	0.70
LF-150606-1	401.46	88.05	6.63	712.01	65.33	121.27	15.12	62.71	12.46	3.88	10.80	1.50
LF-150606-3	349.24	82.27	1.91	647.53	57.50	111.92	14.11	56.72	11.10	3.69	9.75	1.43
Sca-150607-1	393.06	101.69	0.50	1474.42	89.03	159.30	18.31	68.81	11.13	3.20	8.71	1.19
<b>Nova Scotia Dike Samples from Pe-Piper and Reynolds (2000) re-analyzed for this study</b>												
78-19	310.75	92.53	13.12	953.32	61.06	105.25	13.20	56.20	11.61	3.43	9.26	1.30
78-27	230.37	68.45	49.53	627.48	41.35	73.44	8.92	37.03	7.22	2.59	6.83	0.96
78-31B	184.00	47.17	20.10	378.66	32.31	55.39	6.56	26.72	6.36	1.84	5.74	0.86
78-31D	138.27	34.48	346.25	310.19	24.94	46.53	5.56	23.00	5.20	1.72	5.13	0.71
78-31E	181.02	44.27	5.60	376.76	32.82	57.79	7.12	29.64	6.82	1.95	6.32	0.93
78-31H	173.79	42.95	13.55	423.45	30.55	53.22	6.47	27.49	6.17	1.89	5.79	0.85
78-31I	136.55	34.77	13.02	304.33	24.30	44.83	5.34	21.97	4.93	1.63	4.98	0.71
78-31K	174.31	44.17	7.22	356.37	31.61	56.54	6.83	28.54	6.69	2.03	5.79	0.79
78-31M	145.72	36.64	31.04	246.54	26.45	44.67	5.50	22.50	5.47	1.67	5.08	0.74

**Table 3 (cont.): Whole-Rock Trace Element Geochemistry - Method: LA-ICP-MS - Units: PPM**

Sample	Dy	Ho	Er	Tm	Yb	Lu	Hf	Ta	W	Pb	Th	U
<b>CNE Dike Samples from southeast Maine, USA</b>												
BC-01-6-3-2015	5.52	1.04	2.81	0.38	2.38	0.39	6.42	2.82	0.57	9.15	7.48	1.82
BC-02-6-3-2015	4.98	0.92	2.35	0.27	1.87	0.31	3.65	1.82	0.34	2.86	2.56	0.71
BC-03-6-3-2015	4.79	0.86	2.25	0.31	1.86	0.29	3.91	1.34	0.29	3.27	1.97	0.48
BC-04B-6-3-2015	5.06	0.96	2.41	0.29	1.92	0.34	4.44	2.30	0.48	4.67	5.23	1.35
BC-05-6-3-2015	5.73	1.06	2.74	0.35	2.39	0.35	5.12	1.61	0.39	41.95	5.40	1.23
BC-06-6-3-2015	4.62	0.86	2.21	0.31	1.94	0.25	3.12	0.95	0.24	2.61	1.60	0.36
BC-07-6-3-2015	5.38	0.97	2.61	0.35	2.28	0.32	6.64	2.15	0.63	6.36	7.36	1.35
BC-08-6-3-2015	4.19	0.80	2.09	0.28	1.71	0.23	2.94	0.83	0.28	2.71	1.70	0.40
BC-09-6-3-2015	5.02	0.94	2.44	0.31	2.12	0.29	4.81	2.30	0.56	6.23	9.16	1.66
BC-10-6-3-2015	5.28	0.94	2.54	0.35	2.03	0.27	5.15	2.90	0.54	9.50	5.88	1.40
BC-11-6-3-2015	4.96	0.92	2.46	0.34	2.25	0.34	4.32	1.97	0.37	13.07	3.08	0.81
BC-12-6-3-2015	6.22	1.13	3.20	0.42	2.59	0.40	6.62	2.10	0.58	3.73	6.68	1.24
C-1-6-2-2015	6.02	1.15	3.05	0.40	2.41	0.36	4.45	2.09	0.87	16.74	2.23	0.82
C-2-6-2-2015	6.22	1.08	2.67	0.34	1.96	0.27	7.57	5.47	1.08	11.34	9.31	2.31
C-3-6-2-2015	5.59	1.00	2.48	0.30	2.09	0.35	4.98	2.59	19.66	4.95	3.86	1.03
C-4-6-2-2015	4.89	0.91	2.64	0.34	1.98	0.30	4.61	2.25	0.48	2.35	3.58	0.89
C-5-6-2-2015	6.68	1.19	3.17	0.42	2.64	0.39	6.01	3.44	0.62	2.98	3.93	1.27
CAS-1-6-4-2015	6.48	1.16	3.06	0.38	2.45	0.33	6.80	3.03	0.53	16.11	4.57	1.16
CAS-2-6-4-2015	6.87	1.19	2.90	0.40	2.27	0.35	7.12	3.48	0.68	13.40	4.68	1.22
CAS-3-6-4-2015	4.91	0.97	2.46	0.36	2.16	0.35	4.40	2.29	0.51	9.48	4.06	1.02
CAS-4-6-4-2015	5.24	0.90	2.40	0.32	2.19	0.30	6.46	4.32	0.72	5.32	6.23	1.68
CAS-5-6-4-2015	5.21	1.10	2.86	0.37	2.38	0.34	5.21	2.51	0.60	8.90	5.01	1.12
CAS-6-6-4-2015	5.74	1.08	2.64	0.43	2.63	0.42	8.36	5.47	1.03	11.06	9.35	2.58
CAS-7-6-4-2015	9.28	1.87	6.18	0.87	6.88	1.04	24.33	14.86	1.54	15.00	26.36	7.60
CAS-8-6-4-2015	5.33	1.09	3.03	0.48	2.97	0.42	10.72	6.97	1.78	4.54	11.35	3.17
CAS-9B-6-4-2015	5.04	0.99	2.60	0.34	2.17	0.35	3.76	2.20	0.34	2.21	2.79	0.72
COV-1-6-3-2015	4.78	0.84	2.36	0.31	1.92	0.28	3.47	1.93	0.29	3.22	2.66	0.82
COV-2-6-3-2015	5.16	1.01	2.56	0.35	2.01	0.29	4.14	2.31	0.29	2.03	2.86	0.82
Kitt-01-6-2-2015	4.45	0.84	2.15	0.31	1.99	0.28	3.91	1.41	0.96	8.89	2.62	0.76
Kitt-02-6-2-2015	4.80	0.91	2.46	0.31	1.87	0.29	4.12	1.46	1.93	2.39	3.26	0.75
Kitt-03-6-2-2015	5.44	0.96	2.50	0.35	2.00	0.25	4.82	2.72	1.43	8.89	3.58	1.05
Kitt-04-6-2-2015	5.04	0.91	2.29	0.30	1.98	0.26	4.33	2.06	1.45	10.71	3.11	0.93
MIB-1-6-3-2015	6.21	1.10	2.84	0.41	2.34	0.33	5.02	2.12	0.88	3.21	2.83	0.87
MIB-2-6-3-2015	6.71	1.22	3.14	0.43	2.67	0.36	4.84	2.53	0.35	10.20	3.46	0.86
O-1-6-2-2015	7.10	1.27	3.40	0.44	2.82	0.37	8.69	4.32	0.85	20.12	10.43	2.36
O-2-6-2-2015	5.84	1.04	2.61	0.33	2.19	0.29	5.39	3.03	0.69	5.88	4.87	1.30
Port-1B-6-5-2015	3.35	0.65	1.53	0.17	1.20	0.17	3.00	0.68	0.42	11.55	1.41	0.44
SE-1-6-4-2015	6.26	1.17	3.20	0.46	2.99	0.44	7.48	5.17	0.74	5.45	6.23	1.76
Skel-1-6-5-2015	6.29	1.14	2.63	0.32	2.15	0.28	7.72	3.13	0.43	2.46	4.14	1.06
Skel-2-6-5-2015	5.36	1.02	2.78	0.39	2.46	0.34	4.49	1.40	0.34	4.09	3.25	0.62
Skel-3-6-5-2015	4.73	0.92	2.45	0.30	1.85	0.26	3.85	1.32	0.34	4.14	1.95	0.45
Skel-4-6-5-2015	5.37	0.98	2.77	0.37	2.37	0.32	4.99	2.58	0.47	3.09	3.80	0.94
Skel-5-6-5-2015	7.39	1.18	2.95	0.38	2.31	0.30	9.04	3.98	0.56	3.03	4.63	1.11
Skel-6-6-5-2015	4.66	0.91	2.55	0.32	1.88	0.24	3.71	1.06	0.25	3.28	2.14	0.48
<b>Dike Samples from outside CNE area for comparison</b>												
I91-150606-1	4.23	0.74	2.03	0.26	1.67	0.22	2.31	0.94	0.28	2.37	1.27	0.32
LF-150606-1	7.38	1.28	3.37	0.42	2.51	0.32	8.99	5.38	1.46	7.40	6.71	1.79
LF-150606-3	7.02	1.19	3.22	0.37	2.36	0.28	7.80	4.73	1.01	4.76	5.68	1.56
Sca-150607-1	6.86	1.22	3.37	0.47	3.14	0.43	7.32	5.34	1.47	4.38	8.78	2.24
<b>Nova Scotia Dike Samples from Pe-Piper and Reynolds (2000) re-analyzed for this study</b>												
78-19	6.54	1.02	2.60	0.30	2.07	0.24	6.39	5.18	23.69	4.85	7.04	1.75
78-27	4.88	0.83	2.02	0.27	1.52	0.18	4.78	3.77	36.61	3.15	4.91	1.50
78-31B	4.76	0.84	2.13	0.28	1.97	0.22	3.72	2.50	0.52	4.68	4.14	1.06
78-31D	4.01	0.74	1.81	0.23	1.43	0.19	2.89	1.89	0.53	7.43	2.87	0.81
78-31E	5.00	0.87	2.28	0.31	1.80	0.24	3.91	2.54	0.51	4.87	3.91	0.98
78-31H	4.45	0.82	2.06	0.28	1.61	0.23	3.78	2.31	0.51	10.36	3.67	0.93
78-31I	4.02	0.74	1.84	0.25	1.48	0.17	3.06	1.84	0.47	5.88	3.12	0.83
78-31K	4.63	0.80	2.11	0.27	1.77	0.21	3.75	2.32	0.48	6.62	3.64	0.94
78-31M	4.17	0.73	1.90	0.26	1.61	0.19	3.26	1.95	0.49	4.13	3.21	0.80

**Table 4: Whole-Rock Radiogenic Isotope Ratios - Method: TIMS**

Sample	$^{143}\text{Nd}/^{144}\text{Nd}$ 2σ		$^{143}\text{Nd}/^{144}\text{Nd}$ IN	eNd(0)	eNd(t)	$^{176}\text{Hf}/^{177}\text{Hf}$ 2σ		$^{176}\text{Hf}/^{177}\text{Hf}$ IN	eHf(0)	eHf(t)	$^{87}\text{Sr}/^{86}\text{Sr}$ 2σ		$^{87}\text{Sr}/^{86}\text{Sr}$ IN
<b>CNE Dike Samples from southeast Maine, USA</b>													
BC-08-6-3-2015	0.512750	0.000003	0.512476	2.62	2.19	0.282804	0.000004	0.282758	-0.97	0.69	0.704623	0.000006	0.704121
BC-11-6-3-2015	0.512785	0.000003	0.512587	4.79	2.87	0.282812	0.000003	0.282764	-0.74	0.94	0.703823	0.000007	0.703481
C-4-6-2-2015	0.512766	0.000004	0.512558	4.21	2.50	0.282774	0.000003	0.282734	-1.79	-0.39	0.705774	0.000007	0.703973
C-5-6-2-2015	0.512871	0.000004	0.512688	6.76	4.55	0.282871	0.000002	0.282831	1.63	3.04	0.704664	0.000006	0.704177
CAS-4-6-4-2015	0.512823	0.000004	0.512660	6.20	3.60	0.282877	0.000002	0.282849	2.25	3.24	0.703870	0.000008	0.703170
Kitt-03-6-2-2015	0.512828	0.000003	0.512639	5.80	3.70	0.282840	0.000002	0.282808	0.80	1.94	0.704405	0.000005	0.703391
O-1-6-2-2015	0.512649	0.000002	0.512479	2.68	0.21	0.282713	0.000002	0.282687	-3.46	-2.54	0.705968	0.000005	0.705013
SE-1-6-4-2015	0.512802	0.000004	0.512642	5.85	3.19	0.282868	0.000002	0.282832	1.67	2.94	0.703739	0.000008	0.702996
Skel-2-6-5-2015	0.512692	0.000004	0.512469	2.47	1.06	0.282763	0.000003	0.282716	-2.43	-0.77	0.705205	0.000006	0.704019
Skel-5-6-5-2015	0.512827	0.000004	0.512636	5.74	3.68	0.282828	0.000002	0.282808	0.80	1.51	0.703884	0.000006	0.703441
<b>Dike Samples from outside CNE area for comparison</b>													
LF-150606-3	0.512863	0.000004	0.512685	6.70	4.38	0.282858	0.000002	0.282836	1.79	2.57	0.703736	0.000006	0.703315
<b>Nova Scotia Dike Samples from Pe-Piper and Reynolds (2000) re-analyzed for this study</b>													
78-27	0.512830	0.000004	0.512653	6.07	3.74	0.282842	0.000002	0.282819	1.19	2.02	0.705018	0.000008	0.703835

Sample	$^{206}\text{Pb}/^{204}\text{Pb}$ 2σ		$^{206}\text{Pb}/^{204}\text{Pb}$ IN	$^{207}\text{Pb}/^{204}\text{Pb}$	2σ	$^{207}\text{Pb}/^{204}\text{Pb}$ IN	$^{208}\text{Pb}/^{204}\text{Pb}$ 2σ	$^{208}\text{Pb}/^{204}\text{Pb}$ IN	
<b>CNE Dike Samples from southeast Maine, USA</b>									
BC-08-6-3-2015	19.10	0.0004	18.76	15.64	0.0005	15.63	38.992	0.0013	38.514
BC-11-6-3-2015	18.78	0.0004	18.64	15.61	0.0005	15.61	38.587	0.0014	38.409
C-4-6-2-2015	19.59	0.0005	18.69	15.65	0.0004	15.60	39.586	0.0011	38.402
C-5-6-2-2015	20.08	0.0004	19.06	15.66	0.0004	15.61	39.637	0.0012	38.610
CAS-4-6-4-2015	19.42	0.0005	18.67	15.63	0.0005	15.59	39.172	0.0015	38.272
Kitt-03-6-2-2015	18.97	0.0004	18.70	15.64	0.0004	15.63	38.820	0.0010	38.514
O-1-6-2-2015	18.90	0.0005	18.63	15.64	0.0005	15.62	38.876	0.0015	38.482
SE-1-6-4-2015	19.52	0.0004	18.75	15.63	0.0004	15.60	39.188	0.0013	38.308
Skel-2-6-5-2015	19.02	0.0004	18.66	15.64	0.0004	15.62	39.042	0.0012	38.435
Skel-5-6-5-2015	19.76	0.0003	18.88	15.65	0.0004	15.61	39.680	0.0011	38.491
<b>Dike Samples from outside CNE area for comparison</b>									
LF-150606-3	20.14	0.0005	19.35	15.69	0.0004	15.65	39.660	0.0011	38.727
<b>Nova Scotia Dike Samples from Pe-Piper and Reynolds (2000) re-analyzed for this study</b>									
78-27	19.57	0.0004	18.44	15.60	0.0005	15.54	39.260	0.0014	38.057